Circulation Research

ORIGINAL RESEARCH

Nrg1 Regulates Cardiomyocyte Migration and Cell Cycle in Ventricular Development

Joaquim Grego-Bessa, Paula Gómez-Apiñaniz, Belén Prados, Manuel José Gómez, Donal MacGrogan, José Luis de la Pompa

BACKGROUND: Cardiac ventricles provide the contractile force of the beating heart throughout life. How the primitive endocardium-layered myocardial projections called trabeculae form and mature into the adult ventricles is of great interest for biology and regenerative medicine. Trabeculation is dependent on the signaling protein Nrg1 (neuregulin-1). However, the mechanism of action of Nrg1 and its role in ventricular wall maturation are poorly understood.

METHODS: We investigated the functions and downstream mechanisms of Nrg1 signaling during ventricular chamber development using confocal imaging, transcriptomics, and biochemical approaches in mice with cardiac-specific inactivation or overexpression of Nrg1.

RESULTS: Analysis of cardiac-specific *Nrg1* mutant mice showed that the transcriptional program underlying cardiomyocyte-oriented cell division and trabeculae formation depends on endocardial Nrg1 to myocardial ErbB2 (erb-b2 receptor tyrosine kinase 2) signaling and phospho-Erk (phosphorylated extracellular signal-regulated kinase; pErk) activation. Early endothelial loss of Nrg1 and reduced pErk activation diminished cardiomyocyte Pard3 and Crumbs2 (Crumbs Cell Polarity Complex Component 2) protein and altered cytoskeletal gene expression and organization. These alterations are associated with abnormal gene expression related to mitotic spindle organization and a shift in cardiomyocyte division orientation. Nrg1 is crucial for trabecular growth and ventricular wall thickening by regulating an epithelial-to-mesenchymal transition–like process in cardiomyocytes involving migration, adhesion, cytoskeletal actin turnover, and timely progression through the cell cycle G2/M phase. Ectopic cardiac Nrg1 overexpression and high pErk signaling caused S-phase arrest, sustained high epithelial-to-mesenchymal transition–like gene expression, and prolonged trabeculation, blocking compact myocardium maturation. Myocardial trabecular patterning alterations resulting from above- or below-normal Nrg1-dependent pErk activation were concomitant with sarcomere actin cytoskeleton disorganization. The Nrg1 loss- and gain-of-function transcriptomes were enriched for Yap1 (yes-associated protein-1) gene signatures, identifying Yap1 as a potential downstream effector. Furthermore, biochemical and imaging data reveal that Nrg1 influences pErk activation and Yap1 nuclear-cytoplasmic distribution during trabeculation.

CONCLUSIONS: These data establish the Nrg1-ErbB2/ErbB4-Erk axis as a crucial regulator of cardiomyocyte cell cycle progression and migration during ventricular development.

GRAPHIC ABSTRACT: A graphic abstract is available for this article.

Key Words: actin cytoskeleton ■ actins ■ cell cycle ■ endocardium ■ myocardium ■ sarcomeres

In This Issue, see p 883 | Meet the First Author, see p 884

Ventricular chamber development entails transient morphogenetic changes that include the formation of trabeculae, their expansion and growth, and their subsequent incorporation into a compact muscular wall. In zebrafish, trabeculae form by cardiomyocytes extrusion and their radial extension along the inner curvature of the

Correspondence to: Donal MacGrogan, PhD, Intercellular Signalling in Cardiovascular Development & Disease Laboratory, Centro Nacional de Investigaciones Cardiovasculares Carlos III, Melchor Fernández Almagro 3, Madrid 28029, Spain, Email dmacgrogan@cnic.es or José Luis de la Pompa, PhD, Intercellular Signalling in Cardiovascular Development & Disease Laboratory, Centro Nacional de Investigaciones Cardiovasculares Carlos III, Melchor Fernández Almagro 3, Madrid 28029, Spain, Email jlpompa@cnic.es

Supplemental Material is available at https://www.ahajournals.org/doi/suppl/10.1161/CIRCRESAHA.123.323321.

For Sources of Funding and Disclosures, see page 941.

Circulation Research is available at www.ahajournals.org/journal/res

ORIGINAL RESEARCH

Novelty and Significance

What Is Known?

- Myocardial trabeculae play important roles in ventricular chamber growth, development of the conduction system, and formation of the coronary arteries.
- Trabeculae are formed through oriented cell division, and their growth is driven by directional migration.
- The membrane glycoprotein Nrg1 (neuregulin-1) mediates cell-cell signaling and is essential for trabecular development.

What New Information Does This Article Contribute?

- Nrg1 governs a gene expression program involving cardiomyocyte polarity, cell adhesion, actin cytoskeleton dynamics, and mitotic spindle orientation, leading to oriented cell division, trabecular growth, and patterning.
- Nrg1 orchestrates the coordination between cell motility and cell cycle progression, ensuring proper ventricular wall growth.
- Nrg1 is required for the initial growth of the compact myocardium but not for the formation of the coronaries or compaction.
- Ectopic Nrg1 expression results in excessive trabeculation while impairing compaction. This phenotype is accompanied by hypermitogenic cell cycle arrest.
- Nrg1 modulates phospho-Erk (extracellular signal-regulated kinase) and mitosis-associated Yap1 (yes1-associated transcriptional regulator) S274 phosphorylation during trabeculation.

Our study reveals that Nrg1 regulates gene expression related to cardiomyocyte polarity, cell adhesion, actin cytoskeleton dynamics, and mitotic spindle orientation, facilitating oriented cell division and trabecular growth. Nrg1 also coordinates cell motility and cell cycle progression, ensuring proper ventricular wall development without impacting coronary formation or compaction. Aberrant Nrg1 expression leads to excessive trabeculation and compromised compaction, associated with hypermitogenic cell cycle arrest. Our data highlight Nrg1's modulation of specific signals like phospho-Erk and Yap1 S274 phosphorylation during trabeculation. This study illuminates Nrg1's intricate role in heart development, specifically in trabeculation, offering valuable insights into its regulation through cell division and signaling pathways.

Nonstandard Abbreviations and Acronyms

CM	compact myocardium
EMT	epithelial-mesenchymal transition
ErbB2/4	erb-b2 receptor tyrosine kinase 2/4
Erk	extracellular signal-regulated kinase
F-actin	filamentous-actin
pErbB2	phosphorylated erb-b2 receptor tyrosine kinase 2
pErk	phospho-extracellular signal-regulated kinase
pHH3	phospho-histone H3
pYap	phosphorylated Yap
SMA	smooth muscle actin
TM	trabecular myocardium
Yap1	yes1-associated transcriptional regulator

heart and into the ventricular lumen.[1] In mice, trabeculation begins with oriented cell division perpendicular to the ventricular inner wall plane, and trabecular growth is driven by directional migration from the outer (epicardial) layer toward the inner (endocardial) layer.[2] The process of trabeculae coalescence forms a dense meshwork that maximizes ventricular surface area for nutrient and gas exchange in the absence of a coronary circulation.[3] This meshwork later differentiates into a specialized ventricular conduction system and is resolved by expansion of the compact myocardium (CM), with trapped endocardial cells giving rise to the coronary arteries.[4]

Trabecular development requires the signaling activity of the membrane glycoprotein Nrg1 (neuregulin-1).[5] This endocardial protein directly binds to ErbB4 (erb-b2 receptor tyrosine kinase 4) on adjacent cardiomyocytes, triggering ErbB2 (erb-b2 receptor tyrosine kinase 2) ligand–stimulated heterodimerization and tyrosine phosphorylation, followed by downstream pathway activation,[6] including the phospho-Erk (phosphorylated extracellular signal-regulated kinase; pErk) intracellular signaling pathway.[7] Targeted mutation of zebrafish *Erbb2* or *nrg2a*,[8,9] or deletion of mouse *Nrg1*, *ErbB2*, or *ErbB4*,[5,10,11] blocks trabeculation. Cardiomyocyte proliferation and contractility, required for trabeculation, are impaired in mutant *ErbB4* mice[12] and *erbb2* zebrafish,[8] whereas potentiation of ErbB2 signaling in adult mouse cardiomyocytes promotes proliferation and myocardial regeneration.[13] The essential role of Nrg1 in the initiation of trabeculation is well documented, but its role in trabecular growth, maturation, and resolution remains uncertain. In particular, understanding is limited about how morphological transitions occur and progress to yield a mature ventricular wall.

In this study, we used conditional cardiac mutants to demonstrate that Nrg1-induced Erk activation fosters trabecular growth and ventricular wall thickening. This

effect is achieved through the regulation of cell polarity, mitotic spindle orientation, cytoskeletal dynamics, and cell cycle progression. Our analysis revealed significant overlap between Nrg1-dependent genes and those governed by ErbB2 and Lin9, both of which interact with the Hippo pathway, involving Yap1 (yes-associated protein-1). These findings suggest a complex interplay between Nrg1-ErbB2/4-Erk and Hippo-Yap1 signaling, offering promise for future cardiac regeneration therapies.

METHODS

Full Methods are provided in the Supplemental Material.

Data Availability

The authors declare that all supporting data are available within the article and its Supplemental Material.

RESULTS

Nrg1-ErbB2/4-pErk Signaling in Trabeculae Growth

We used *Nrg1*^{flox} mice[14] and the *Tie2*^{Cre} driver line[15] to inactivate *Nrg1* in endothelial and endocardial cells starting from E7.5 (Methods). E8.5 control and *Nrg1*^{flox};*Tie2*^{Cre} embryos both showed a bilayered myocardial epithelium (Figure S1A and S1C). E9.5 controls displayed nascent trabeculae and a double-layered CM (Figure 1A; Figure S1B), whereas *Nrg1*^{flox};*Tie2*^{Cre} mutants had fewer trabecular projections and thicker CM (Figure 1B and 1C; Figure S1D). E10.5 control trabeculae became more complex, whereas *Nrg1*^{flox};*Tie2*^{Cre} mutants had rudimentary trabeculae and thicker CM (Figure S1E through S1H). Three-dimensional reconstructions confirmed differences in CM thickness and trabecular network size and complexity (Figure 1D through 1F; Figure S1I and S1J; Videos S1 and S2). E9.5 *Nrg1*^{flox};*Tie2*^{Cre} hearts had reduced endocardial Nrg1 expression (Figure 1G and 1H) and weak myocardial expression of phosphorylated ErbB2 (pErbB2; Figure 1I and 1J) and pErk (Figure 1K through 1M). *Nrg1*^{flox};*Tie2*^{Cre} embryos did not survive beyond E12.5 (Table S1, sheet 1).

We examined *Nrg1* transcription during cardiac development by in situ hybridization. At E10.5, *Nrg1* was transcribed throughout the endocardium (Figure S2A). Between E12.5 and E16.5, it persisted in scattered endocardial cells (Figure S2B through S2E). We also assessed pErk expression as an Nrg1-pErbB2 activity readout[13] (Figure S2F through S2J). From E9.5 to E11.5, pErk was detected in the myocardium, particularly at trabeculae tips (Figure S2F and S2G). At E12.5, pErk expression shifted to the base of trabeculae (Figure S2H), suggesting involvement in endocardium-derived coronary vessels development. At E13.5, pErk was detected in a few myocardial cells and nascent coronaries (Figure S2I). At E16.5, pErk expression was mostly restricted to coronary endothelium (Figure S2J). pErk expression is consistent with an Nrg1 role in trabecular myocardium (TM) between E9.5 and E12.5 and in coronary endothelium thereafter.

Nrg1 Requirement for Cardiac Developmental Patterning and Proliferation

We examined the ECM (extracellular matrix), required for cardiomyocyte migration and trabeculae formation.[16] At E8.5, Alcian blue staining revealed ECM glycosaminoglycans in control and *Nrg1*^{flox};*Tie2*^{Cre} hearts (Figure S3A and S3C). At E9.5 and E10.5, staining was reduced in *Nrg1*^{flox};*Tie2*^{Cre} hearts (Figure S3B through S3F), indicating a trabeculation defect.

RNA sequencing analysis of E9.5 identified 1219 differentially expressed genes ($P<0.05$; Table S2, sheets 1 and 2) between control and *Nrg1*^{flox};*Tie2*^{Cre} hearts. Mutant hearts showed reduced expression of *Nrg1* and key trabecular genes, including *Bmp10*, *Hand1*, *Irx3*, and *Sema3a* (Figure 1N and 1O; Figure S3I through S3L). Additionally, Has2, involved in cardiac jelly synthesis,[16] was decreased and limited to rudimentary trabeculae (Figure 1N; Figure S3G and S3H). Itgα6 (integrin alpha 6) expression was also reduced in *Nrg1*^{flox};*Tie2*^{Cre} mutants (Figure S3M through S3O). In contrast, *Hey2* transcription increased in the CM of *Nrg1*^{flox};*Tie2*^{Cre} mutants (Figure 1O), indicating disruption in trabeculation and chamber myocardium patterning due to Nrg1-ErbB2/4 signaling abrogation.

Enrichment analysis of HALLMARK gene sets (false discovery rate, $q<0.05$),[17] uncovered cellular stress pathways (HYPOXIA and REACTIVE_OXYGEN_SPECIES; Figure 1P), associated with p53 activation (Figure 1P). The leading-edge genes of the P53_PATHWAY were related to cell cycle, DNA damage response, apoptosis, and p53 response processes (Figure S4A).[18] Other enriched pathways included proliferation and growth (ESTROGEN_RESPONSE_EARLY, MYC_TARGETS_V2, MTORC1_SIGNALING, and E2F_TARGETS; Figure 1P; Table S2, sheet 3), with E2F_TARGETS representing genes involved in cell cycle regulation, chromatin homeostasis, DNA repair and replication, mitosis, and cytoskeletal regulation (Figure S4B). To elucidate this defect, we measured bromodeoxyuridine (BrdU) incorporation as an S-phase marker from E8.5 and E10.5 (Figure 1Q; Figure S5). At E8.5, proliferation was similar in control and *Nrg1*^{flox};*Tie2*^{Cre} hearts (Figure S5A, S5B, and S5E). However, at E9.5, there was a 10% reduction in proliferation in the CM of *Nrg1*^{flox};*Tie2*^{Cre} hearts (Figure S5C through S5E). This difference persisted in E10.5 CM but not in the endocardium or TM (Figure 1Q and 1S). Examination of E2F_TARGET genes revealed increased expression of cell cycle inhibitors, including p21/*Cdkn1a*, p27/*Cdkn1b*, p18/*Cdkn2c*, and CIP2/*Cdkn3* (Figure S4). *Cdkn1b*

ORIGINAL RESEARCH

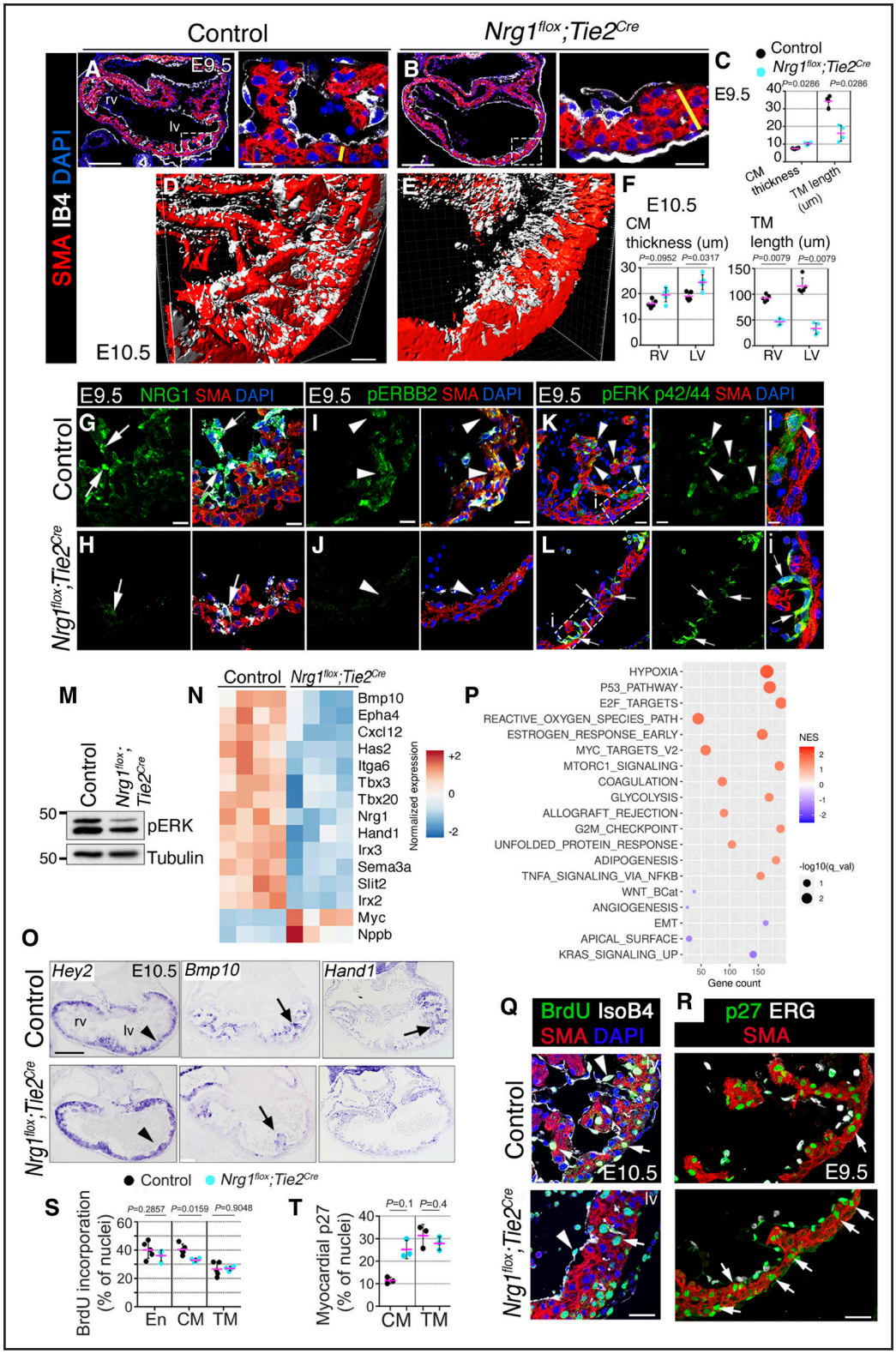

Figure 1. Nrg1 (neuregulin-1)-ErbB2 (erb-b2 receptor tyrosine kinase 2)- phospho-Erk (phosphorylated extracellular signal-regulated kinase; pErk) signaling requirement for trabeculation initiation and expansion.

Immunofluorescence (IF) against SMA (smooth muscle actin; red) and IB4 (isolectin B4; white) in sections from E9.5 control (**A**) and *Nrg1*^{flox};*Tie2*^{Cre} hearts (**B**). Yellow lines mark compact myocardium (CM) thickness. DAPI counterstained (blue). **C**, Quantification of CM thickness and trabecular myocardium (TM) length in E9.5 control and *Nrg1*^{flox};*Tie2*^{Cre} left ventricles (n=4 embryos per genotype, ≥3 sections per embryo). **D** and **E**, Three-dimensional reconstruction of SMA-stained E10.5 control and *Nrg1*^{flox};*Tie2*^{Cre} left ventricles. **F**, Quantifications of CM thickness and TM length (n=7 embryos per genotype, ≥3 sections per embryo). **G** through **L**, IF for Nrg1, pErbB2, and pErk in E9.5 control (**G**, **I**, and **K**) and *Nrg1*^{flox};*Tie2*^{Cre} embryos (**H**, **J**, and **L**). SMA, red; IB4, white. DAPI counterstained. Arrows mark endocardium; arrowheads mark (*Continued*)

encodes for cyclin-dependent kinase inhibitor p27^{Kip1} protein, which binds and blocks cyclin-CDK to arrest the cell cycle and organismal growth.[19] Consistent with reduced BrdU measurements, p27 protein expression was increased in *Nrg1*^{flox};*Tie2*^{Cre} CM but did not change in TM (Figure 1R and 1T).

Pathways previously linked to trabeculation in zebrafish,[1] such as KRAS_SIGNALING_UP, APICAL_SURFACE, and epithelial-to-mesenchymal transition (EMT), were also affected (Figure 1P; Figure S4C and S4D; Table S2, sheet 3). These processes, involving the cytoskeleton, cellular motility, and ECM, tended to be depleted (false discovery rate, q<0.5; Figure 1P; Figure S4C and S4D). Overall, our data indicate that Nrg1-ErbB2/4 signaling is required for both patterning and emergence of trabeculae, and CM cardiomyocyte proliferation. Despite reduced proliferation, cardiomyocytes contributing to trabeculae formation remained within the myocardium of *Nrg1*^{flox};*Tie2*^{Cre} mutants, resulting in abnormal ventricular thickening.

Nrg1 Requirement for Polarity Gene Expression and Cytoskeletal Organization

Cell polarity and cytoskeletal dynamics are interlinked processes implicated in altered trabeculation in mice and zebrafish.[1,20] Genes associated with cytoskeletal actin remodeling (*Arf4*, *Dock2*, *Sh3bp1*, and *Arf6*) and organization (*Rac1* and *Rac2*), cell polarity (*Amotl1*, *Pard3*, *Nek3*, *Dlg1*, *Sipa1l3*, *Stk11*, and *Wnt11*), cell division orientation (*Sapcd2*), motility (*Kif26b* and *Actr2*), and Fgf-Erk signaling (*Spry2* and *Fgf10*) were dysregulated in *Nrg1*^{flox};*Tie2*^{Cre} hearts (Figure 2A).

In E8.5 controls, filamentous-actin (F-actin) staining showed even circumferential distribution at the plasma membrane (Figure 2B and 2C; Videos S3 and S5), while *Nrg1*^{flox};*Tie2*^{Cre} hearts exhibited nonuniform F-actin distribution concentrated at cell junctions (Figure 2B and 2C; Videos S4 and S6), indicating the disruption of the actin cortical network. This defect was consistent with the aberrant expression of gene sets related to cytoskeleton (Gene Ontology [GO]: 0005856) and regulation of actin polymerization (GO: 0008064) in *Nrg1*^{flox};*Tie2*^{Cre} mutants (Figure S6A and S6B).

Nrg1^{flox};*Tie2*^{Cre} hearts displayed reduced *Pard3* (Par-3 Family Cell Polarity Regulator; Figure 2A; Table S2, sheet 2). *Pard3* inactivation disrupts apicobasal polarity in epithelial cells[21] and causes planar polarity defects in endothelial cells.[22] En face immunofluorescence staining of Pard3 in E8.5 control hearts showed even distribution at the apical/abluminal pole of ventricular cardiomyocytes (Figure 2D, left; Figure 2E). However, Pard3 was diminished in *Nrg1*^{flox};*Tie2*^{Cre} hearts (Figure 2D, right; Figure 2E). While E8.5 and E9.5 control cardiomyocytes exhibited Pard3 at the apical/abluminal pole (Figure 2F), it was notably lacking in trabecular cardiomyocytes (Figure S7A, S7C, and S7C'), aligning with loss of apicobasal polarity in these cells.[1] In contrast, Pard3 was severely depleted in E8.5 and E9.5 *Nrg1*^{flox};*Tie2*^{Cre} ventricles (Figure 2F; Figure S7B, S7D, and S7D'), suggesting altered apicobasal cardiomyocyte polarity. Crumbs2 (Crumbs Cell Polarity Complex Component 2)—essential for cardiomyocyte apicobasal polarity in zebrafish[23]—was located at the apical pole of E8.5 control CM cardiomyocytes (Figure S7E and S7F) but was depleted in *Nrg1*^{flox};*Tie2*^{Cre} mutants (Figure S7G and S7H), indicating a potential loss of polarity in *Nrg1*^{flox};*Tie2*^{Cre} cardiomyocytes. Thus, loss of Nrg1 is linked to decreased expression of cell polarity proteins and actin cytoskeleton disorganization.

Nrg1 Requirement for Oriented Division During Trabeculation

The interaction between polarity complexes and the cytoskeleton determines mitotic spindle positioning and cell division orientation.[24] Abnormal expression of genes related to mitotic spindle assembly, such as *Cep250*, *Aurka*, *Katnb1*, *Dlg1*, *Tubgcp2*, *Kif1b*, and *Kif5b*, was observed in *Nrg1*^{flox};*Tie2*^{Cre} mutants (Figure 2G). Moreover, spindle orientation during trabeculation has been linked to the function and cellular distribution of adhesion complexes.[25] Additionally, alterations in adhesion molecules were indicated by changes in cell adhesion (GO: 0007155) and regulation of cell-matrix adhesion (GO: 0001952) gene sets (Figure S6C and S6D). These data support Nrg1-ErbB2-pERK signaling requirement in gene regulation of cell polarity, adhesion, and spindle orientation during trabeculation.

Figure 1 Continued. myocardium. **M**, Western blot of pErk in E9.5 ventricles (pool of n=3 per genotype). **N**, Heatmap of differentially expressed genes (DEGs) in E9.5 control vs *Nrg1*^{flox};*Tie2*^{Cre} hearts. The color code represents normalized gene expression from −2 to +2. **O**, *Hey2*, *Bmp10*, and *Hand1* in situ hybridization (ISH) in E9.5 control and *Nrg1*^{flox};*Tie2*^{Cre} embryos. Arrows, TM; arrowheads, CM. **P**, Gene set enrichment analysis (GSEA) for E15.5 *Nrg1*^{flox};*Tie2*^{Cre} vs control against Hallmark gene sets. The bubble plot represents enrichment data for a selection of 19 Hallmark gene sets at false discovery rates (FDRs) of q<0.1 and q<0.5, for gene sets with positive or negative enrichment score, respectively. Scale bar indicates normalized enrichment score (NES) from −2 to +2. Gene count is the number of genes at the intersection between the complete collection of genes used as input for the analysis and the complete list of genes included in the gene set, according to the corresponding database. **Q**, Bromodeoxyuridine (BrdU) IF in E10.5 control and *Nrg1*^{flox};*Tie2*^{Cre} embryos. Arrows, myocardium; arrowheads, endocardium. **R**, p27 IF in E9.5 control and *Nrg1*^{flox};*Tie2*^{Cre} embryos. Arrows, myocardium. **S**, Quantification of BrdU incorporation in E10.5 control (n=5, ≥3 sections per embryo) and *Nrg1*^{flox};*Tie2*^{Cre} embryos (n=4, ≥3 sections per embryo). **T**, Quantification of p27 IF in E9.5 control and *Nrg1*^{flox};*Tie2*^{Cre} embryos (n=3 embryos per genotype). *P* values obtained by the Mann-Whitney *U* test. Scale bars, 200 µm (low magnification in **A**, **B**, and **O**), 50 µm (**D** and **E**), 20 µm (high magnification in **A**, **B**, and **G** through **L**, **Q**, and **R**), and 10 µm (high magnification in **Gi** and **Hi**). En indicates endocardium; LV, left ventricle, and RV, right ventricle.

ORIGINAL RESEARCH

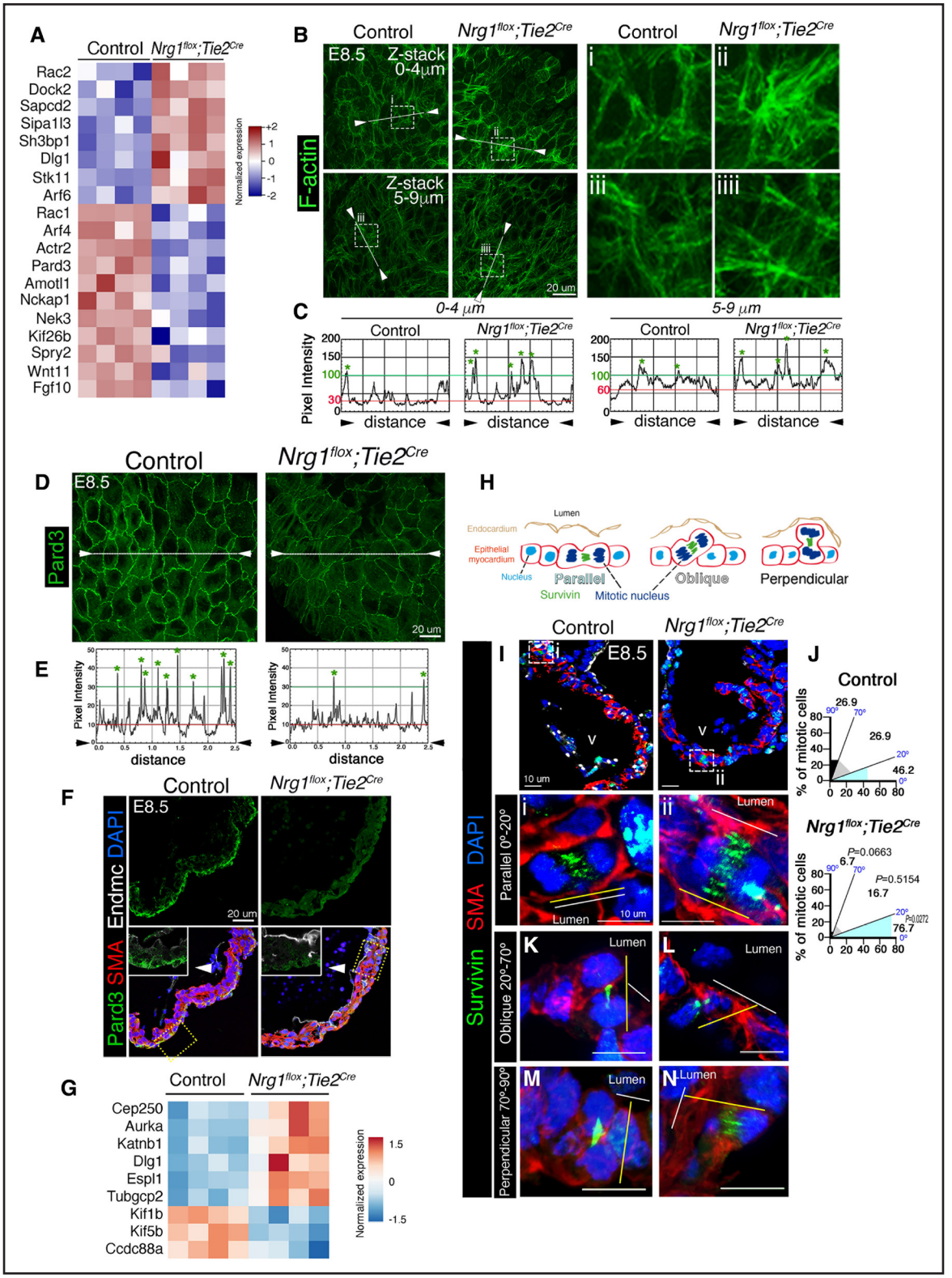

Figure 2. Nrg1 (neuregulin-1) requirement for polarity gene expression and cytoskeletal organization during trabeculation. **A**, Panther enrichment analyses of 1219 differentially expressed genes (DEGs) in *Nrg1*^{flox};*Tie2*^{Cre} vs control comparison identified establishment or maintenance of cell polarity (Gene Ontology [GO]: 0007163) as enriched (*P*=0.0064). Heatmap shows relative expression of DEGs associated with this GO term. **B**, Whole-mount phalloidin staining Z-stack projections of apical (0–4 μm) and basolateral (5–9 μm) regions of outer compact myocardium (CM) in E8.5 control and *Nrg1*^{flox};*Tie2*^{Cre} heart sections. **C**, Pixel intensity quantification along a 10-pixel-wide trace (white lines in **B**). Red lines indicate similar background intensities in control and *Nrg1*^{flox};*Tie2*^{Cre} heart sections. Green asterisks indicate values above gray intensity of 100 (green lines). **D**, Whole-mount immunofluorescence (IF) for Pard3 (Par-3 Family Cell Polarity Regulator). **E**, Pixel intensity quantification along a 10-pixel-wide trace (white lines between arrowheads). Red lines indicate similar background intensities in control and (*Continued*)

Cardiomyocytes divide obliquely or perpendicular to the lumen to form the nascent trabeculae, whereas those that divide in parallel contribute to the CM[2,20] (Figure 2H). Survivin immunofluorescence allows visualization of the mitotic cleavage furrow and division axis during telophase (Figure 2I and 2J; Figure S7I through S7O). In E8.5 controls, 46.2% cardiomyocyte mitosis were parallel (between 0° and 20°) to the ventricular lumen (Figure 2I, i and 2J), 26.9% were oblique (between 20° and 70°; Figure 2J and 2K), and 26.9% were perpendicular (between 70° and 90°; Figure 2J and 2M). In somite-matched E8.5 *Nrg1*^{flox};*Tie2*^{Cre} mutants, parallel divisions significantly increased (76.7%; Figure 2I, ii and 2J), with reductions in oblique (16.7%; Figure 2J and 2L) and perpendicular divisions (6.7%; Figure 2J and 2N). In E9.5 controls, parallel divisions still prevailed (61.4%) compared with perpendicular (14%) and oblique divisions (24.6%; Figure S7I, S7K, S7M, and S7O). Yet, in E9.5 *Nrg1*^{flox};*Tie2*^{Cre} mutants, up to 83.6% of divisions were parallel, 14.5% were oblique (Figure S7J, S7L, and S7O), and perpendicular divisions dropped to 1.8% (Figure S7N and S7O). Thus, cardiomyocyte-oriented cell division is disrupted in *Nrg1*^{flox};*Tie2*^{Cre} mutants. Biased parallel division in *Nrg1*^{flox};*Tie2*^{Cre} mutants might offset the observed reduction of proliferation at E9.5, leading to increased CM thickness.

Nrg1 Requirement for Ventricular Wall Formation but Not Coronary Development

To bypass *Nrg1*^{flox};*Tie2*^{Cre} lethality (Table S1, sheet 1), we bred *Nrg1*^{flox} and *Cdh5*^{CreERT2} mice[26] to generate mice with inducible pan-endothelial *Nrg1* deletion. Administering consecutive 4-hydroxytamoxifen doses at E10.5 and E11.5 inhibited TM and CM growth in E13.5 *Nrg1*^{flox};*Cdh5*^{CreERT2} mice (Figure S8A and S8B), resulting in thinner TM and CM at E16.5 (Figure 3A through 3C). Altered expression of the ventricular conduction system, trabecular and CM markers *Gja5*, *Bmp10*, and *Hey2*, revealed loss of trabeculae patterning and CM expansion in mutants (Figure 3D; Figure S8C through S8F). *Nrg1*^{flox};*Cdh5*^{CreERT2} mice survived until E18.5 (Table S1, sheet 2). Later, 4-hydroxytamoxifen induction (E12.5–E13.5) did not cause ventricular abnormalities at E18.5 (Figure S8G through S8K), indicating that Nrg1-pErk requirement precedes E13.5.

We performed RNA sequencing on E15.5 control and *Nrg1*^{flox};*Cdh5*^{CreERT2} hearts (Table S3, sheets 1 and 2). Differentially expressed genes (Benjamini-Hochberg [B-H], $P<0.05$) were associated with angiogenesis, migratory processes (*Cxcr4*, *Vegfb*, *Aplnr1*, *Edn1*, *Ednrb*, and *Angpt1*; Figure 3E), and ventricular conduction system development (*Sema3a*, *Efna1*, *Nkx2-5*, *Etv1*, and *Ache*; Figure 3E). In mice, coronary arteries are located deep within the myocardial wall, whereas the veins are superficial, beneath the epicardium.[27] The organization and complexity of coronary arteries, as well as the venous tree organization, were unaffected in E16.5 *Nrg1*^{flox};*Cdh5*^{CreERT2} mutant hearts (Figure S9A, S9B, S9D, S9E, S9F, and S9H). Similar results were obtained with the vascular endothelial-specific *Pdgfb*^{iCreERT2} Cre driver line[28] (Figure S9C, S9D, S9G, and S9H).

Further in situ hybridization for coronary veins (*CoupT-FII*), arteries (*Dll4*), coronaries (*Fapbp4*), and endothelial markers (*Cdh5*) in E16.5 *Nrg1*^{flox};*Cdh5*^{CreERT2} mutants and control littermates did not reveal discernible differences (Figure S9I through S9P). To assess the relative number of endothelial cells in the E16.5 heart's CM, we quantified IB4 (isolectin B4)-positive signal percentage but found no distinction between *Nrg1*^{flox};*Cdh5*^{CreERT2} and controls (Figure S10A through S10C), indicating the absence of coronary vascular defects in *Nrg1* mutants. Furthermore, SM22 (smooth muscle cell-specific cytoskeletal protein) and Notch3 immunofluorescence showed unaffected coronary vessel smooth muscle cell differentiation and pericyte coverage in *Nrg1*^{flox};*Cdh5*^{CreERT2} hearts (Figure S10D and S10E). Thus, lack of an inner compact wall does not affect coronary development in *Nrg1*^{flox};*Cdh5*^{CreERT2} hearts, suggesting that any reduced endocardial contribution to coronary vasculogenesis in these mutants is compensated for by alternative endothelial cells sources.

Nrg1 Regulates Motility and G2/M Progression During Ventricular Wall Growth

Further analysis identified depleted HALLMARK gene set was EMT (−log[false discovery rate], $P<0.05$; Figure 3F; Table S3, sheet 3). The leading-edge depleted genes were associated with cell cytoskeleton, ECM composition, and adhesion molecules (Figure S11A and S11B). Other depleted gene sets evoked cell shape and polarity (APICAL_SURFACE and APICAL_JUNCTION) and promigratory signaling pathways (WNT_BETA_CATENIN_SIGNALING and HEDGEHOG_SIGNALING; Figure 3F). Furthermore,

Figure 2 Continued. *Nrg1*^{flox};*Tie2*^{Cre} heart sections. Green asterisks represent values above gray intensity of 30 (green lines). **F**, Pard3 IF in transverse sections of E8.5 control and *Nrg1*^{flox};*Tie2*^{Cre} embryos (green). Arrowheads in insets mark the apical domain of the CM. DAPI counterstained (blue). **G**, Heatmap of DEGs for components and mitotic spindle regulators. Color code represents normalized gene expression from −1.5 to +1.5. **H**, Schematic of mitotic spindle orientation analysis relative to the cardiac lumen: parallel (0°–20°), oblique (20°–70°), or perpendicular (70°–90°). **I** through **N**, Representative IF images of mitotic cells stained for survivin (green) and SMA (smooth muscle actin; red) in control and *Nrg1*^{flox};*Tie2*^{Cre} heart sections at E8.5. DAPI counterstained. A general view of E8.5 hearts is shown in the **top** (**I**, insets **i** and **ii**). White lines in **i** and **ii** and **K** through **N** indicate the reference plane of the cardiac lumen. Yellow lines indicate mitotic spindle orientation. **J**, OCD quantification in E8.5 control (n=3 embryos; n=26 mitotic figures) and *Nrg1*^{flox};*Tie2*^{Cre} hearts (n=3 embryos; n=30 mitotic figures). *P* values obtained by Fisher exact test. $P<0.05$. Scale bars, 20 µm (**B**, **D**, and **F**), 15 µm (**D**), and 10 µm (**I**–**N**).

ORIGINAL RESEARCH

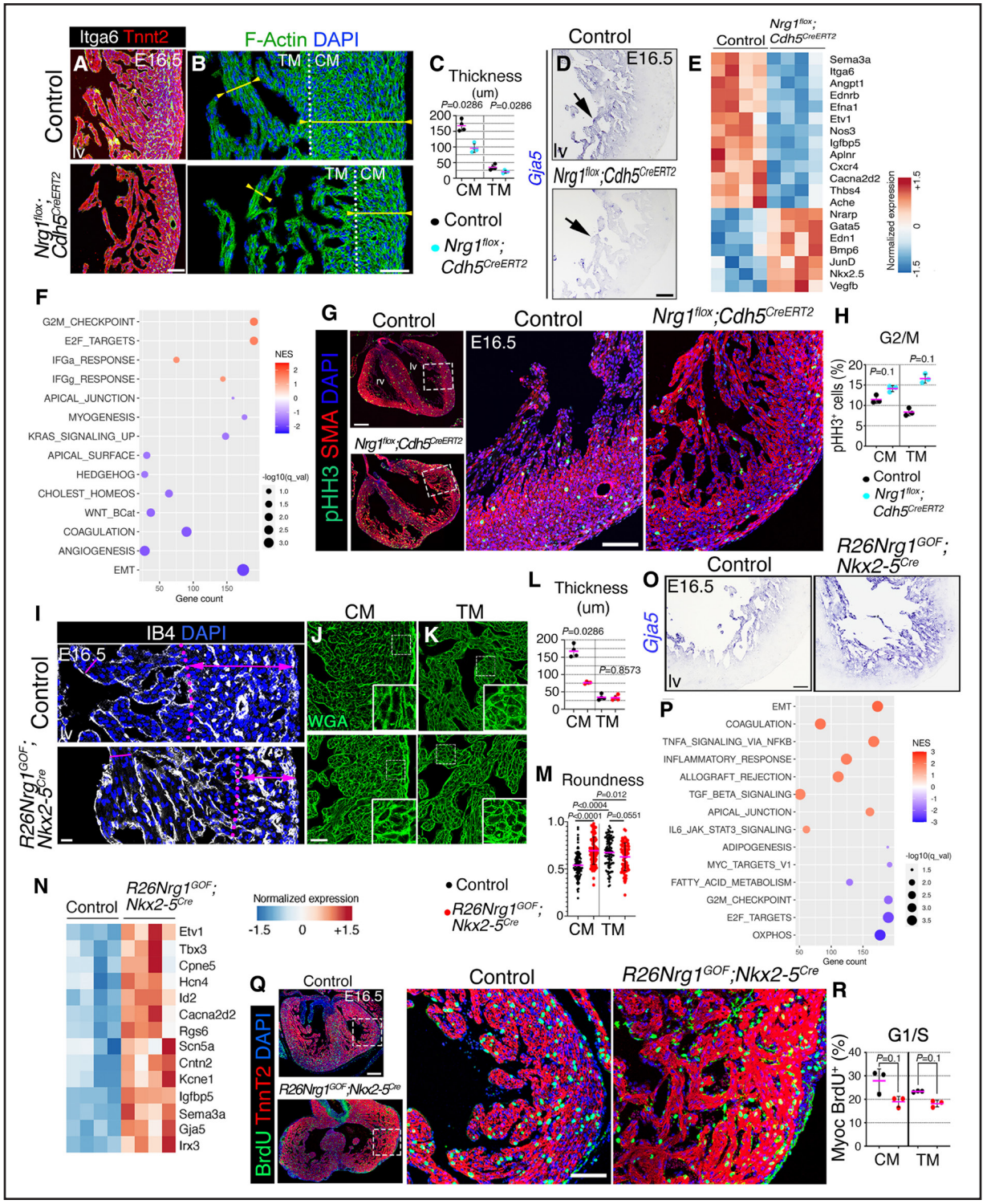

Figure 3. Nrg1 (neuregulin-1) role in trabecular growth and inner ventricular wall formation.
A and **B**, Itga6 (integrin α6) and Tnnt2 (troponin T2) immunofluorescence (IF; **A**) and phalloidin (F-actin; **B**) staining in E16.5 control and *Nrg1*^{flox};*Cdh5*^{CreERT2} heart sections. Dotted lines mark the compact myocardium (CM)–trabecular myocardium (TM) separation. **C**, Quantification of CM and TM thickness (n=4 embryos per genotype and ≥3 sections per embryo). **D**, *Gja5* ISH in E16.5 control and *Nrg1*^{flox};*Cdh5*^{CreERT2} embryos. Arrows mark TM. **E**, Heatmap of representative differentially expressed genes (DEGs) in E15.5 control vs *Nrg1*^{flox};*Cdh5*^{CreERT2} hearts. The color code represents normalized gene expression from −1.5 to +1.5. **F**, Gene set enrichment analysis (GSEA) for E15.5 *Nrg1*^{flox};*Cdh5*^{CreERT2} vs control against Hallmark gene sets. The bubble plot represents enrichment data for a selection of 14 Hallmark gene sets with false discovery rate (FDR) q<0.25. Scale bar indicates normalized enrichment score (NES) from −2 to +2. Gene count is the number of genes at the intersection between the complete collection of genes used as input for the analysis and the complete list of genes included in the gene set, according to the corresponding database. **G**, **Left**, Phospho-histone 3 (pHH3) IF on E16.5 control and *Nrg1*^{flox};*Cdh5*^{CreERT2} heart sections (n=3 per genotype). **G**, **Right**, Boxed regions magnified. **H**, Quantification of %pHH3^{+} cardiomyocytes (n=3 per genotype and ≥3 sections per embryo). **I**, (*Continued*)

CHOLESTEROL_HOMEOSTASIS depletion aligns with Nrg1-ErbB4's role in cholesterol metabolism.[29] Conversely, overrepresented pathways like G2/M_CHECKPOINT and E2F_TARGETS point to a proliferative defect (Figure 3F), involving associated cell cycle, chromatin, DNA repair, replication, and mitosis-related genes (Figure S11C), whereas nuclear transport and transcription regulation pathways and, importantly, the cytoskeleton (Figure S11B and S11C) emphasize the nucleus-cytoskeleton connection.

We examined E16.5 *Nrg1*^{flox}*;Cdh5*^{CreERT2} mutants for changes in the G1/S and G2/M cell cycle phases using BrdU incorporation and the mitosis marker phosphohistone H3 (pHH3). At E16.5, these mutants showed a higher proportion of pHH3-positive (pHH3^{+}) cardiomyocytes, especially in TM (Figure 3G and 3H), and this difference was already noticeable at E12.5 (Figure S12A, S12B, and S12R). There was no change in the proportion of BrdU^{+} cells in CM or TM, either at E13.5 (Figure S12C, S12D, and S12G) or at E16.5 (Figure S12E, S12F, and S12G). Ki67 staining, which marks the S-G2 phases, also confirmed that Nrg1 depletion did not affect proliferation at E12.5 or E16.5 (Figure S12H through S12K and S12R). These findings suggest that *Nrg1* mutants experience a delay or prolongation in cell cycle progression through the G2/M phase, while the G1/S phase remains unaffected.

We examined p27^{Kip1} protein expression, known both as a pERK effector[30] and a cell cycle regulator.[31] At E12.5, p27 expression increased in *Nrg1*^{flox}*;Cdh5*^{CreERT2} CM and TM (Figure S12L, S12M, and S12R), aligning with elevated pHH3 and a potential G2/M delay. This difference persisted in CM at E16.5, although p27 staining was greatly reduced in both control and mutant by then (Figure S12N through S12Q and S12R). This analysis indicates that Nrg1 regulates trabecular growth and chamber formation by coordinating cell migration and G2/M progression.

Ectopic Nrg1 Expression Induces Trabeculation

For further insight, we generated a transgenic line bearing a *Rosa26-floxNeoSTOPflox-Nrg1-eGFP* expression cassette (Figure S13A and S13B; Methods). Nkx2-5^{Cre}-mediated[32] removal of the Neo-STOP sequences led to the expression of both GFP (Figure S13C and S13D) and Nrg1 (Figure S13E and S13F). E16.5 *R26Nrg1*^{GOF}*;Nkx2-5*^{Cre} hearts were developmentally arrested, resembling E12.5 controls (Figure S14A and S14B). This was evident in the presence of a double-outlet right ventricle, overriding aorta (Figure S14A), and ventricular septal defect (Figure S14B). Additionally, E16.5 *R26Nrg1*^{GOF}*;Nkx2-5*^{Cre} hearts exhibited superficial outgrowths resembling fistulae (Figure S14Ci and S14Cii), likely due to direct communication between the endocardium and epicardium caused by CM thinning (Figure 3I and 3L). *R26Nrg1*^{GOF}*;Nkx2-5*^{Cre} mice die by E18.5 (Table S1, sheet 3).

At E16.5, transgenic epicardium had 3 to 4 cell layers instead of one (Figure S14D). The subepicardial layer had infiltrated endothelial cells but lacked coherent large vessel conduits (Figure 3I; Figure S14D). Cardiomyocyte shape (roundness) in the outer CM of *R26Nrg1*^{GOF}*;Nkx2-5*^{Cre} hearts resembled control TM more than the corresponding CM (Figure 3J, 3K, and 3M). Additionally, Itgα6 expression expanded in E10.5 *R26Nrg1*^{GOF}*;Nkx2-5*^{Cre} hearts from TM to CM (Figure S14E and S14F). Thus, Nrg1 overexpression transforms CM into trabecular like.

RNA sequencing analysis on E15.5 transgenic hearts identified >4500 differentially expressed genes in *R26Nrg1*^{GOF}*;Nkx2-5*^{Cre} hearts (false discovery rate, $q<0.05$; Table S4, sheets 1 and 2). As expected, the expression of a subset of His-Purkinje–specific genes[33] was upregulated (Figure 3N). In situ hybridization revealed expanded *Gja5* transcription toward the CM (Figure 3O), consistent with the role of Nrg1 as a ventricular conduction system differentiation driver.[34] Gene set enrichment analysis revealed the enrichment for promigratory processes (EMT, APICAL_JUNCTION, and KRAS_SIGNALING_UP) in *R26Nrg1*^{GOF}*;Nkx2-5*^{Cre} hearts (Figure 3P), involving expression of the EMT transcription factors *Snail* and *Twist* (Figure S15A; Table S4, sheets 2 and 3) and EMT signaling pathways, including TGFβ (TGF_BETA_SIGNALING) and BMP (Figure 3P; Figure S15B and S15C; Table S4, sheets 2 and 3).

Conversely, metabolic pathways (OXPHOS, FATTY_ACID_METABOLISM, and ADIPOGENESIS), associated

Figure 3 Continued. IB4 (isolectin B4) and DAPI staining in E16.5 control and *R26Nrg1*^{GOF}*;Nkx2-5*^{Cre} transverse heart sections. Double-headed arrows indicate myocardium thickness. Dotted lines demark the CM-TM separation. **J** and **K**, WGA (wheat germ agglutinin)-FITC staining on transverse sections of CM and TM in E16.5 control and *R26Nrg1*^{GOF}*;Nkx2-5*^{Cre} hearts. Quantification of CM and TM thickness (**L**) and cell roundness (**M**) in E16.5 control and *R26Nrg1*^{GOF}*;Nkx2-5*^{Cre} heart sections (n=3 embryos per genotype and ≥3 sections per embryo). **N**, Heatmap of DEG in E15.5 *R26Nrg1*^{GOF}*;Nkx2-5*^{Cre} vs control hearts. The color code represents NES from −1.5 to +1.5. **O**, *Gja5* ISH in E16.5 control and *R26Nrg1*^{GOF}*;Nkx2-5*^{Cre} hearts. **P**, GSEA for E15.5 *R26Nrg1*^{GOF}*;Nkx2-5*^{Cre} vs control against Hallmark gene sets. The bubble plot represents enrichment data for a selection of 14 Hallmark gene sets with FDR $q<0.05$. Scale bar indicates NES from −3 to +3. Gene count is the number of genes at the intersection between the complete collection of genes used as input for the analysis and the complete list of genes included in the gene set, according to the corresponding database. **Q**, **Left**, Bromodeoxyuridine (BrdU)-positive IF on E16.5 control and *R26Nrg1*^{GOF}*;Nkx2-5*^{Cre} hearts (n=3 per genotype). **Q**, **Right**, Boxed regions magnified. **R**, Quantification of %BrdU incorporation in CM and TM in control and *R26Nrg1*^{GOF}*;Nkx2-5*^{Cre} hearts (n=3 per genotype and ≥3 sections per embryo). *P* values obtained by the Mann-Whitney *U* test. Scale bars, 100 μm in **A**, **D**, and **O**; 50 μm in **B**; 200 μm in **G**; 50 μm in **G**, inset; 20 μm in **I** through **K**; 200 μm in **Q**; and 50 μm in insets. lv, left ventricle

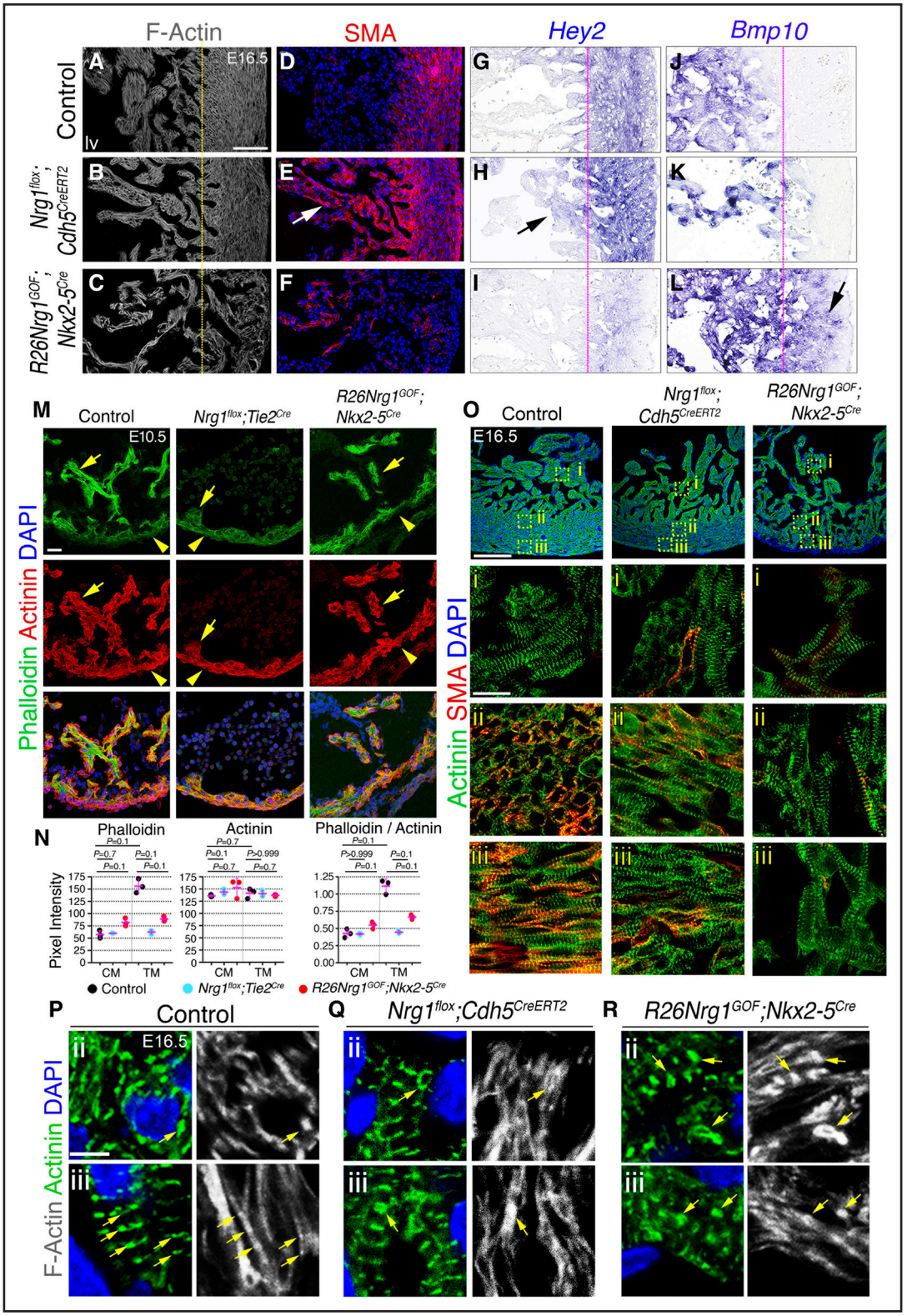

Figure 4. Cytoskeletal dynamics mediate ventricular patterning.
A through **F**, Phalloidin (filamentous-actin [F-actin]) staining and SMA (smooth muscle actin) immunofluorescence (IF) in E16.5 left ventricular sections from control (**A** and **D**), *Nrg1*^{flox};*Cdh5*^{CreERT2} (**B** and **E**), and *R26Nrg1*^{GOF};*Nkx2-5*^{Cre} hearts (**C** and **F**). Yellow lines mark the position of the trabecular myocardium (TM)–compact myocardium (CM) morphological border. The border shifts in *Nrg1*^{flox};*Cdh5*^{CreERT2} and *R26Nrg1*^{GOF};*Nkx2-5*^{Cre} hearts. The arrow marks strong SMA immunostaining in TM relative to CM in *Nrg1*^{flox};*Cdh5*^{Cre} hearts (**E**). Note also reduced SMA expression in *R26Nrg1*^{GOF};*Nkx2-5*^{Cre} CM (**F**). **G** through **L**, *Hey2* and *Bmp10* ISH in E16.5 left ventricular sections from control (**G** and **J**), *Nrg1*^{flox};*Cdh5*^{CreERT2} (**H** and **K**), and *R26Nrg1*^{GOF};*Nkx2-5*^{Cre} hearts (**I** and **L**). Pink lines mark the position of the TM-CM morphological border. The border shifts in *Nrg1*^{flox};*Cdh5*^{CreERT2} and *R26Nrg1*^{GOF};*Nkx2-5*^{Cre} hearts. Arrows mark ectopic *Hey2* and *Bmp10* expression in *Nrg1*^{flox};*Cdh5*^{CreERT2} and (*Continued*)

with MYC activity (MYC_TARGET_V1 and MYC_TARGET_V2; Figure 3P; Table S4, sheets 2 and 3), were depleted, revealing impaired cardiac metabolic maturation. Intermediate filament genes have been implicated in lineage determination and organ maturation.[35] *Lamins*, *nestin*, and *keratin* genes were differentially regulated in *R26Nrg1*^{GOF}*;Nkx2-5*^{Cre} hearts (Figure S15D). In E16.5 controls, Nestin expression was weak in TM but strong in endothelium and epicardium (Figure S14Gi and S14Gi'). In contrast, *R26Nrg1*^{GOF}*;Nkx2-5*^{Cre} hearts displayed Nestin expression in TM and in the expanded subepicardium, devoid of SMA (smooth muscle actin) staining (Figure S14Hii and S14Hii'). Overall, Nrg1 overexpression alters the relative proportion of ventricular wall cell types and causes the CM to become trabecular-like

Ectopic Nrg1 Expression Causes Cell Cycle Arrest and a Prosenescence Phenotype

The metabolic defect was also associated with upregulation of cytotoxic stress, proinflammatory, and prosenescence gene sets (Figure 3P; Figure S15E and S15F; Table S4, sheet 3). Activation of cellular stress pathways suppresses cell division and promotes senescence and has been associated with hypermitotic cell cycle arrest.[36] Indeed, depletion of cell cycle–related gene sets (E2F_TARGETS and G2M_CHECKPOINT; Figure 3P) suggested a proliferation defect. We examined E12.5 and E16.5 *R26Nrg1*^{GOF}*;Nkx2-5*^{Cre} hearts for cell cycle alterations. The proportion of BrdU^{+} cells was lower in both the CM and TM of E16.5 *R26Nrg1*^{GOF}*;Nkx2-5*^{Cre} hearts (Figure 3Q and 3R), suggesting reduced proliferation or delayed G1/S progression. This was confirmed by Ki67 staining (Figure S16A through S16D). However, pHH3^{+} indexes in CM were unaffected in E12.5 and E16.5 *R26Nrg1*^{GOF}*;Nkx2-5*^{Cre} hearts (Figure S16E, S16F, and S16I). In TM, pHH3^{+} staining increased at E12.5 but not at E16.5 (Figure S16E, S16F, and S16I). These findings suggest reduced ventricular wall proliferation in *R26Nrg1*^{GOF}*;Nkx2-5*^{Cre} hearts, aligning with the suggested trabeculation of the CM.

Analysis of E2F_TARGET genes revealed changes in key cell cycle regulators, with increased *cdkn1a*/p21 and decreased *cdkn1b*/p27, *cdkn2c*/p18 (Figure S15G), potentially contributing to the growth delay. p27 expression was higher in both CM and TM of *R26Nrg1*^{GOF}*;Nkx2-5*^{Cre} hearts (Figure S16G and S16I), correlating with reduced BrdU labeling (Figure 3Q and 3R) and a potentially delayed G1/S phase. *Cdkn1b* transcription did not match protein expression, likely due to posttranscriptional regulation of p27.[37] Increased p27 expression persisted in CM but not TM at E16.5 (Figure S16H and S16I). These data indicate that Nrg1 overexpression promotes cell cycle arrest and a prosenescence phenotype.

Nrg1 Regulates Ventricular Patterning Mediated by Cytoskeletal Dynamics

TM and CM marker analysis in *Nrg1*^{flox}*;Cdh5*^{CreERT2} and *R26Nrg1*^{GOF}*;Nkx2-5*^{Cre} hearts revealed changes in ventricular patterning (Figure 4A through 4L). At E16.5, SMA typically marks immature proliferative CM[38] (Figure 4D). However, in *Nrg1*^{flox}*;Cdh5*^{CreERT2} hearts, SMA extended along the trabeculae (Figure 4E), indicating defective maturation and expanded CM identity. Conversely, SMA was reduced in the CM of *R26Nrg1*^{GOF}*;Nkx2-5*^{Cre} hearts (Figure 4F), indicating loss of CM identity and acquisition of a trabecular one. In support, in situ hybridization showed *Hey2* expression abnormally extended into TM of *Nrg1*^{flox}*;Cdh5*^{CreERT2} hearts, contrasting its normal CM restriction (Figure 4G and 4H), and was almost absent from *R26Nrg1*^{GOF}*;Nkx2-5*^{Cre} ventricles (Figure 4G and 4I), reflecting loss of CM identity. In contrast, *Bmp10* transcription was reduced in TM of *Nrg1*^{flox}*;Cdh5*^{CreERT2} mutants (Figure 4J and 4K) and extended into CM in *R26Nrg1*^{GOF}*;Nkx2-5*^{Cre} embryos (Figure 4J and 4L), reflecting acquisition of TM identity. In summary, Nrg1 loss of function leads to a compact-like TM, while Nrg1 gain of function results in a trabecular-like CM.

Tissue patterning partly relies on the cytoskeleton.[39] We investigated actin cytoskeleton changes possibly contributing to patterning defects by analyzing F-actin (phalloidin) and α-actinin (Figure 4M through 4O). In E10.5 controls, phalloidin staining was notably higher in TM compared with CM, while α-actinin showed similar intensity (Figure 4M and 4N). However, phalloidin staining in TM was similar to CM in E10.5 *Nrg1*^{flox}*;Tie2*^{Cre} mutants, and CM staining resembled TM in E10.5 *R26Nrg1*^{GOF}*;Nkx2-5*^{Cre} hearts (Figure 4M and 4N). This indicated that the contrast in F-actin staining intensity, characteristic of TM and CM, disappeared in both *Nrg1*^{flox}*;Tie2*^{Cre} and *R26Nrg1*^{GOF}*;Nkx2-5*^{Cre} hearts, in line with the loss of TM and CM identities. Immunofluorescence against α-actinin (Figure 4O) showed that the sarcomeres in trabecular cardiomyocytes of E16.5 control, *Nrg1*^{flox}*;Cdh5*^{CreERT2}, and *R26Nrg1*^{GOF}*;Nkx2-5*^{Cre} hearts displayed well-organized striation pattern (Figure 4Oi). In

Figure 4 Continued. *R26Nrg1*^{GOF}*;Nkx2-5*^{Cre} hearts. Note also reduced *Hey2* expression in CM of *R26Nrg1*^{GOF}*;Nkx2-5*^{Cre} hearts. **M**, F-actin (phalloidin) and α-actinin staining in E10.5 control, *Nrg1*^{flox}*;Tie2*^{Cre}, and *R26Nrg1*^{GOF}*;Nkx2-5*^{Cre} hearts. Yellow arrows, TM; arrowheads, CM. **N**, Quantification of phalloidin and α-actinin staining and phalloidin/α-actinin ratios in heart sections from E10.5 control, *Nrg1*^{flox}*;Cdh5*^{CreERT2}, and *R26Nrg1*^{GOF}*;Nkx2-5*^{Cre} embryos (n=3 embryos per genotype and 4 measurements per embryo). *P* values were obtained by the Mann-Whitney *U* test. **O**, α-Actinin and α-SMA immunodetection in E16.5 control, *Nrg1*^{flox}*;Cdh5*^{CreERT2}, and *R26Nrg1*^{GOF}*;Nkx2-5*^{Cre} hearts. **i**, **ii**, and **iii** show high-magnification views of TM, inner CM, and outer CM, respectively. **P** through **R**, Detail of F-actin and α-actinin double IF at E16.5 in inner CM (**ii**) and outer CM (**iii**). Yellow arrows mark Z bands and highlight aberrant Z-band structures in *Nrg1*^{flox}*;Cdh5*^{CreERT2} and *R26Nrg1*^{GOF}*;Nkx2-5*^{Cre} hearts. Scale bars, 100 μm in **A** through **I**, and **O**; 20 μm in **M**; 10 μm in **Oi** through **Oiii**; and 5 μm in **P** through **R**.

ORIGINAL RESEARCH

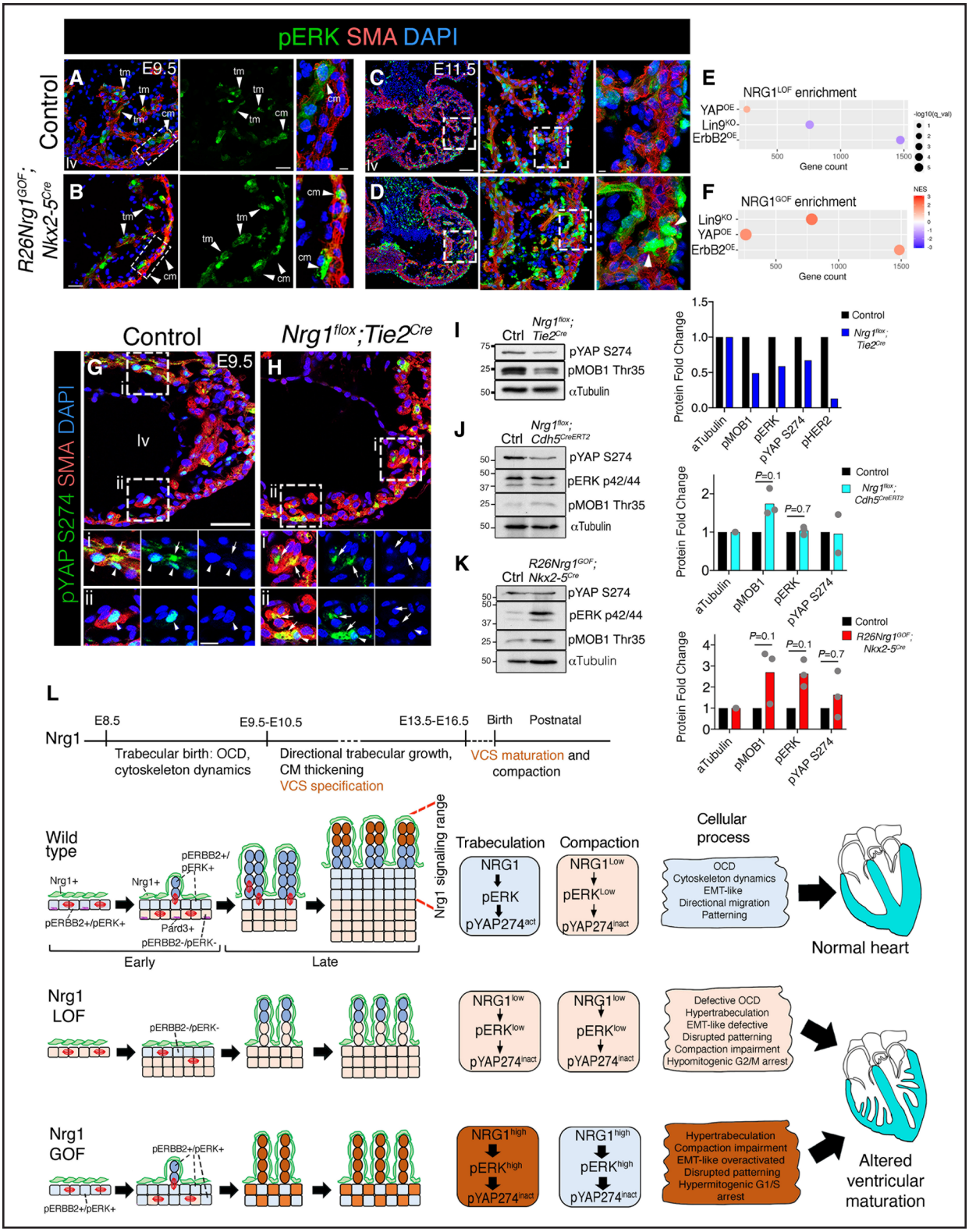

Figure 5. Nrg1 (neuregulin-1)-mediated phospho-Erk (extracellular signal-regulated kinase; pErk) and phosphorylated Yap1 (yes1-associated transcriptional regulator; pYap1) regulation in chamber development.

A through **C**, pErk immunofluorescence (IF) in E9.5 (**A** and **B**) and E11.5 embryos (**C** and **D**). Arrowheads indicate labeled cardiomyocytes in trabecular myocardium (TM) and compact myocardium (CM). **E** and **F**, Gene set enrichment analysis (GSEA) for E15.5 *Nrg1*^{flox}*;Cdh5*^{CreERT2} vs control (**E**) and *R26Nrg1*^{GOF}*;Nkx2-5*^{Cre} vs control (**F**), against gene sets of ERBB2^{OE} vs control and Lin9^{KO} vs control, or direct YAP1 target genes. Bubble plots showing enrichment data at false discovery rate (FDR) q<0.25, with color scale indicating NES from −3 to +3. **G**, pYAP S274 IF in E9.5 control and (**H**) *Nrg1*^{flox}*;Tie2*^{Cre} heart sections. Arrows mark cytoplasmic signal, and arrowheads mark nuclear signal. **I**, Western blot analysis and quantification of pYAP S274 and pMOB1-Thr35 in E9.5 control and *Nrg1*^{flox}*;Tie2*^{Cre} ventricles (pool of n=3 per genotype), (*Continued*)

control CM, cardiomyocytes had 2 distinct fiber patterns: inner CM with circular striation (Figure 4Oii) and outer CM with fiber orientation similar to TM (Figure 4Oiii). Sarcomere fiber orientation in *Nrg1^{flox};Cdh5^{CreERT2}* hearts was defective in the inner CM (and similar to the outer CM), while the outer CM remained normal (Figure 4Oii and 4Oiii). Conversely, CM in *R26Nrg1^{GOF};Nkx2-5^{Cre}* ventricles had sarcomere fiber orientation resembling TM (Figure 4Oi through 4Oiii). *Nrg1^{flox};Cdh5^{CreERT2}* CM showed diffuse sarcomeres with ring-like structures (Figure 4P, 4Qii, and 4Qiii), suggesting disrupted Z-line alignment. This striated sarcomere structure was also evident in F-actin staining, with ring-like structures in *Nrg1^{flox};Cdh5^{CreERT2}* hearts (Figure 4Qii and 4Qiii), indicating misalignment of F-actin branching. Similar ring-like structures were observed in CM sarcomeres of *R26Nrg1^{GOF};Nkx2-5^{Cre}* hearts (Figure 4Rii and 4Riii). Thus, altered Nrg1 expression disrupts ventricular patterning and is associated with changes in F-actin organization and sarcomere Z-line positioning.

Nrg1 Modulates pErk-Dependent Yap1 S274 Phosphorylation During Trabeculation

pErk expression in developing hearts is a Nrg1 signaling readout (Figure 1K through 1M; Figure S2F and S2G). In E9.5 control hearts, pErk was expressed in trabeculae and nearby (Figure 5A) and in some epicardial cells at E11.5 (Figure 5C). In contrast, E9.5 to E11.5 *R26Nrg1^{GOF};Nkx2-5^{Cre}* hearts showed ectopic pErk expression in CM and subepicardial layers (Figure 5B and 5D). From E13.5 onward, pErk was absent in control myocardium (Figure S2I and S2J) but present in coronary endothelial cells (Figure S17A), akin to *Nrg1^{flox};Cadh5^{CreERT2}* hearts (Figure S17B). By E16.5, ectopic pErk expression in *R26Nrg1^{GOF};Nkx2-5^{Cre}* myocardium has subsided (Figure S17C).

We examined pErbB2 and pErbB4 expression during compaction. In E16.5 controls, pErbB2 and pErbB4 were expressed in coronary endothelium, sparsely in endocardium, and absent from myocardium (Figure S17D and S17G). pErbB2 was also found in epicardium (Figure S17D). In *Nrg1^{flox};Cadh5^{CreERT2}* hearts, coronary endothelial and endocardial expression persisted (Figure S17E and S17H). In *R26Nrg1^{GOF};Nkx2-5^{Cre}* hearts, pErbB2 and pErbB4 were expressed in both endothelium and endocardium but remained absent from myocardium (Figure S17F and S17I). Thus, during compaction, myocardial expression of pErbB2 and pErbB4 diminishes, and Nrg1 cannot induce their expression in this tissue.

The *R26Nrg1^{GOF};Nkx2-5^{Cre}* gene signature closely mirrored those found in adult mouse hearts overexpressing ErbB2 (ErbB2^{OE})[40] and in fetal hearts deficient for the activator MuvB core complex component Lin9 (Lin9^{KO}, [41]; Figure S17J and S17K). Notably, the EMT and OXPHOS gene signatures were respectively enriched and depleted in the 3 transcriptomes, whereas the opposite change occurred after Nrg1 inactivation (Figure 3F; Figure S17L). ErbB2-mediated cardiac regenerative effects involve Yap1,[40] and there was significant overlap between the Yap1-regulated and Lin9-dependent gene signatures.[42] Gene set enrichment analysis revealed that many differentially expressed genes in ErbB2^{OE} and Lin9^{KO} hearts exhibited significant alterations in the Nrg1 transcriptomes (Figure 5E and 5F; Figure S17L). Moreover, the E15.5 *R26Nrg1^{GOF};Nkx2-5^{Cre}* transcriptome displayed significant overlap with the Yap1 target gene signature[43] (Figure S18A), potentially linking Yap1 downstream of Nrg1-pERK in the signaling cascade.

ErbB2 signaling via Erk elicits cytoskeletal changes with an altered mechanical state and downstream Yap S274 phosphorylation, resulting in phosphorylated Yap (pYap) activation and nuclear localization.[40] Given the enrichment of Yap1 target genes in *R26Nrg1^{GOF};Nkx2-5^{Cre}* hearts, we examined the Nrg1 mutants for Hippo (Mob1)-dependent Yap1 phosphorylation on S112 (S127 in human) and pErk and mitosis-associated Yap1 phosphorylation on S274 (S289 in human).[44] Control E9.5 expressed pYap S112 in the cytoplasm of endocardial cells and weakly in some cardiomyocytes (Figure S18B). In *Nrg1^{flox};Tie2^{Cre}* hearts, pYap S112, while maintained in the endocardium, was not visible in cardiomyocytes (Figure S18C). pMob1-Thr35 expression was also below normal (Figure 5I), suggesting

Figure 5 Continued. pYAP S274, pERK 42/44, and pMOB1-Thr35 in E16.5 control and *Nrg1^{flox};Cdh5^{CreERT2}* (**J**), and control and *R26Nrg1^{GOF};Nkx2-5^{Cre}* ventricles (**K**). n=1 embryo per genotype; n=2 to 3 replicas (**J** and **K**). *P* values were obtained by the Mann-Whitney *U* test. α-Tubulin was used as gel-loading control and for normalization in quantifications. Scale bars: 100, 20, and 10 µm in **A** and **B** (low- to high-magnification view); 100, 30, and 10 µm in **C** and **D**; 50 um in **G** and **H**; 10 um in **i** and **ii**. **L**, Proposed Nrg1 function in ventricular chamber development and maturation. E8.5 to E10.5: wild type, Nrg1 released from the endocardium (green) activates phosphorylated ErbB2 (erb-b2 receptor tyrosine kinase 2; pErbB2) and pErk in TM (blue), promoting nuclear pYap S274 (pYap S274^{act}). Signaling involves actin cytoskeleton activation, apical-basal (A-B) polarity loss, epithelial-mesenchymal transition (EMT)–like phenotype, OCD, directional migration, and patterning (CM vs TM). Nrg1 loss of function (LOF; E8.5–E10.5): disrupted Nrg1 signaling affects OCD, causing CM thickening and underdeveloped trabeculae, associated with A-B polarity marker depletion, disorganized actin cytoskeleton, low pErk, and pYap S274 inactivation (pYap S274^{inact}). E10.5 to E16.5: wild-type trabeculae elongate via directional migration from outer CM (beige) to inner CM (blue). Nrg1 is crucial for ventricular conduction system (VCS) specification (brown) but not compaction. Nrg1 LOF (E10.5–E16.5) results in Nrg1 depletion, low pErk, and TM expressing CM genes, leading to rudimentary mispatterned trabeculae, reduced inner myocardial wall growth, and hypomitogenic cell cycle arrest. Nrg1 gain of function (GOF; E10.5–E16.5), cardiac Nrg1 overexpression, high pErk, trabeculation of CM, and impaired compaction. Hypermitogenic signaling causes cell cycle arrest and senescence onset. Both Nrg1 LOF and GOF disrupt ventricular chamber maturation and cardiac developmental progress.

that Hippo-dependent Yap1 nuclear localization would be higher in E9.5 *Nrg1*^{flox};*Tie2*^{Cre} hearts. However, at E13.5, pYap S112 was found exclusively in endocardial cells in both control and *Nrg1*^{flox};*Cadh5*^{CreERT2} hearts (Figure S18D and S18E), and the same restriction was observed at E16.5 in control and *R26Nrg1*^{GOF};*Nkx2-5*^{Cre} hearts (Figure S18F and S18G). Thus, pYap S112 expression and Hippo-regulated Yap activity are dependent on Nrg1 at E9.5 but independent of Nrg at E13.5 or E16.5.

In E9.5 controls, pYap S274 was localized in cardiomyocyte nuclei (Figure 5G) but was mostly cytoplasmic in *Nrg1*^{flox};*Tie2*^{Cre} hearts (Figure 5H). In agreement, Western blot revealed below-control pYap S274 expression in *Nrg1*^{flox};*Tie2*^{Cre} hearts (Figure 5I). Consistent with the dependence of pYap S274 on Erk phosphorylation.[40] pErk expression was also below control (Figure 1M). In contrast, at E16.5, pYap S274 immunofluorescence labeled only scattered cells in the myocardium of control, *Nrg1*^{flox};*Cdh5*^{CreERT2}, and *R26Nrg1*^{GOF};*Nkx2-5*^{Cre} hearts (Figure S18H through S18J), although Western blot detected above control-level expression of pMob1-Thr35 in both Nrg1 loss-of-function and gain-of-function mutants (Figure 5J and 5K). These data suggest that Erk phosphorylation, pYap S274 cellular distribution, and Hippo/Mob1 activity in cardiomyocytes are dependent on Nrg1 during trabeculation but not during compaction.

DISCUSSION

Trabeculation is a dynamic process, involving transient disruption of the myocardial cell layer integrity and a distribution of polarized morphologies and division dynamics across the ventricles (Figure 5L). In zebrafish, this manifests as an EMT-like process involving actin cytoskeleton changes, resulting in actomyosin polarization, apical constriction, depolarization, and delamination without division.[1,8,45] In mice, realignment of the division axis of cardiomyocytes undergoing trabeculation involves transient disruption and repositioning of polarity, focal cell, and matrix adhesion complexes.[2,20] Spindle orientation and directional migration are guided by intracellular signaling cascades, which shape the contractile actomyosin network and impact force transmission.[24]

We demonstrate that Nrg1 regulates gene expression crucial for cell shape and morphology, including key polarity complex components, with depletion of the apical junction and polarity proteins Pard3 and Crumbs2, related with oriented cell division and trabeculation[20,23] (Figure 5L). These changes were also linked to ventricular wall defects and modified expression of cell junction components essential for myocardial structural integrity.[2,25] Disrupted actin organization in *Nrg1*^{flox};*Tie2*^{Cre} cardiomyocytes causes a failure to acquire the motile and invasive behaviors required for correct orientation of the mitotic spindle and orthogonal cardiomyocyte division. Later, trabecular growth relies on EMT-like migration of cardiomyocytes from the outer compact layer to the trabeculae (Figure 5L).

Initial thickening of the inner myocardial wall depends on the formation of a mixed trabecular/compact zone near the source of Nrg1. The outer CM starts with 2 to 3 layers but attains a thickness of about 15 to 20 cell layers by the end of trabeculation (Figure 5L), likely through differential growth.[46] The inner CM may serve as a feeder for trabecular growth,[2] consistent with studies identifying migrating cell clones spanning transmural locations during chamber development.[2,47] These EMT-like processes disrupt cell-cell interactions and polarity complexes, accompanied by actin filament rearrangement to bestow invasive behaviors required for cellular motility.[48] However, they occur without canonical EMT transcription factors or mesenchymal marker acquisition, suggesting a partial or incomplete EMT.[48] Thus, Nrg1 regulates CM and TM spatial distribution by generating molecularly distinct myocardial layers and establishing trabecular boundaries (Figure 5L).

Therefore, Nrg1 promotes TM and inner CM development while limiting the growth of outer CM proliferative cardiomyocytes. Analogously to lung airway epithelium,[49] parallel cardiomyocyte division may represent the default orientation for myocardial growth. Nrg1-ErbB2/4-Erk signaling might act as a switch to override this default orientation, not by offering an orientation cue but by determining a cell's responsiveness to such cues. Cell polarity pathways, vital for spindle angle control in epithelial tissues, may fulfill these roles.[24] Besides transcriptional regulation, an Nrg1-pErbB2/4-pErk kinase cascade may also impact centrosomal components or cytoskeletal elements that control centrosome position and spindle orientation.[50]

Nrg1 overexpression profoundly alters CM cellular composition, increasing endothelial and epicardial cell proportions compared with cardiomyocytes. This suggests that, as development proceeds, patterning and growth of the outer CM no longer depends on Nrg1, as cardiomyocytes lose sensitivity to endocardial signals, and pErk downstream effector activity is suppressed in the myocardium, likely through ErbB2/4 downregulation. This aligns with a limited spatiotemporal role during the trabeculation phase of ventricular development. Due to their higher proliferation rate, CM cardiomyocytes eventually outgrow trabecular cardiomyocytes during compaction.[51] TM versus CM specification could hinge on cardiomyocyte proximity to Nrg1's source, with its impact primarily affecting endocardial-proximal cardiomyocytes responsible for subendocardial ventricular myocardium and Purkinje fibers.[33] (Figure 5L).

Our studies highlight the coordination between cell division and migration in shaping tissue growth and morphogenesis patterns and boundaries.[52] Nrg1 not only impacts morphogenesis and EMT-like processes but also regulates genes related to cell cycle progression,

including mitosis, DNA processes, and the cytoskeleton.[53] The link between cytoskeleton organization, cell adhesion, and the cell cycle[54] is evident in actin-regulated G2/M checkpoint mechanisms.[55] Our interpretation that Nrg1-pErk signaling is required for G2/M phase progression aligns with earlier research highlighting ERBB2 (HER2) and ERK1/2 as key regulators of the G2/M checkpoint response to genotoxic stress.[56] Two types of cell cycle arrest are highlighted here[36]: (1) classical (hypomitogenic) growth arrest caused by growth factor withdrawal, resulting in cell cycle exit characterized by inactivation of both upstream (Ras-Mapk signaling) and downstream proliferation factors; (2) hypermitogenic cell cycle arrest, resulting from active mitogen-activated pathways and impaired cell cycle progression, leading to a senescence-like phenotype.

The available evidence indicates that (1) Nrg1 activates endogenous ErbB4 to induce Yap1 target genes in breast cancer cells[29]; (2) ErbB2 drives mitosis during cardiac regeneration via pErk-dependent Yap1 activation[40]; (3) interaction of Yap1 with the Myb-MuvB complex promotes mitotic gene expression in fetal cardiomyocytes[41]; and (4) Yap1-driven cardiac regeneration relies on the transcription of cell cycle, adherens-junction, and cytoskeletal genes.[43,57,58] Given the significant overlap involving EMT-like genes between Nrg1, ErbB2 and Yap1 gain-of-function, and Lin9 inactivation gene signatures, and Nrg1 requirement for Yap1 S274 nuclear localization during trabeculation (but not during compaction), Yap1 could act as an Nrg1 downstream effector during trabeculation (Figure 5L)

Trabeculation defects, reduced intertrabecular spacing, and underdeveloped CM are key morphological features of left ventricular noncompaction cardiomyopathy.[59] Experimental human cell data suggest that left ventricular noncompaction cardiomyopathy may result from faulty cardiomyocyte proliferation.[60] In contrast, mouse data indicate that the persistence of postnatal trabeculae could be attributed to either excessive TM proliferation[61] or reduced CM proliferation.[51] Our studies suggest that left ventricular noncompaction cardiomyopathy could be associated with disrupted asymmetrical growth and differentiation throughout the ventricular wall, resulting in defective trabecular patterning and cardiomyocyte proliferation. The extensive overlap of cell division and morphogenesis complicates distinguishing their separate roles in TM and CM growth. The potential for multiomic measurement at a single-cell level offers an exciting opportunity for future research.

ARTICLE INFORMATION

Received July 3, 2023; revision received October 6, 2023; accepted October 10, 2023.

Affiliations

Intercellular Signalling in Cardiovascular Development & Disease Laboratory, Centro Nacional de Investigaciones Cardiovasculares Carlos III (CNIC), Madrid, Spain (J.G.-B., P.G.-A., B.P., D.M., J.L.d.l.P.). CIBER de Enfermedades Cardiovasculares, Madrid, Spain (J.G.-B., P.G.-A., B.P., D.M., J.L.d.l.P.). Bioinformatics Unit, CNIC, Madrid, Spain (M.J.G.).

Acknowledgments

The authors thank A. Galicia and L. Méndez for mouse husbandry, Centro Nacional de Investigaciones Cardiovasculares Carlos III Genomics Unit for RNA sequencing, and S. Bartlett for English editing.

Sources of Funding

This study was supported by grants PID2019-104776RB-I00 and PID2020-120326RB-I00, CB16/11/00399 (Centro de investigación Biomédica en Red Cardiovascular [CIBER CV]) from Ministerio de Ciencia e Innovación (MCIN)/Agencia Española de Investigación (AEI)/10.13039/501100011033, Fundación Banco Bilbao Vizcaya Argentaria (BBVA; reference number: BIO14_298), Fundació La Marató de TV3 (reference number: 20153431), and the Spanish Society for Cardiology (SECSCFG-INV-CFG 21/004) to J.L. de la Pompa. J. Grego-Bessa was funded by Programa Atracción de Talento from Comunidad de Madrid (reference number 2016T1/BMD1540). Support for this publication also came from the European Regional Development Fund. The Centro Nacional de Investigaciones Cardiovasculares Carlos III (CNIC) is supported by the Instituto de Salud Carlos III (ISCIII), MCIN, and the Pro-CNIC Foundation and is a Severo Ochoa Center of Excellence (grant CEX2020001041-S) financed by MCIN/AEI/10.13039/501100011033.

Disclosures

None.

Supplemental Material

Expanded Materials & Methods
Figures S1–S18
Videos S1–S6
Tables S1–S5
Major Resources Tables
References 62–70

REFERENCES

1. Jimenez-Amilburu V, Rasouli SJ, Staudt DW, Nakajima H, Chiba A, Mochizuki N, Stainier DY. In vivo visualization of cardiomyocyte apicobasal polarity reveals epithelial to mesenchymal-like transition during cardiac trabeculation. *Cell Rep.* 2016;17:2687–2699. doi: 10.1016/j.celrep.2016.11.023
2. Li J, Miao L, Shieh D, Spiotto E, Li J, Zhou B, Paul A, Schwartz RJ, Firulli AB, Singer HA, et al. Single-cell lineage tracing reveals that oriented cell division contributes to trabecular morphogenesis and regional specification. *Cell Rep.* 2016;15:158–170. doi: 10.1016/j.celrep.2016.03.012
3. Sedmera D, Pexieder T, Vuillemin M, Thompson RP, Anderson RH. Developmental patterning of the myocardium. *Anat Rec.* 2000;258:319–337. doi: 10.1002/(SICI)1097-0185(20000401)258:4<319::AID-AR1>3.0.CO;2-O
4. Wu B, Zhang Z, Lui W, Chen X, Wang Y, Chamberlain AA, Moreno-Rodriguez RA, Markwald RR, O'Rourke BP, Sharp DJ, et al. Endocardial cells form the coronary arteries by angiogenesis through myocardial-endocardial VEGF signaling. *Cell.* 2012;151:1083–1096. doi: 10.1016/j.cell.2012.10.023
5. Meyer D, Birchmeier C. Multiple essential functions of neuregulin in development. *Nature.* 1995;378:386–390. doi: 10.1038/378386a0
6. Sanchez-Soria P, Camenisch TD. ErbB signaling in cardiac development and disease. *Semin Cell Dev Biol.* 2010;21:929–935. doi: 10.1016/j.semcdb.2010.09.011
7. Baliga RR, Pimental DR, Zhao YY, Simmons WW, Marchionni MA, Sawyer DB, Kelly RA. NRG-1-induced cardiomyocyte hypertrophy. Role of PI-3-kinase, p70(S6K), and MEK-MAPK-RSK. *Am J Physiol.* 1999;277:H2026–H2037. doi: 10.1152/ajpheart.1999.277.5.H2026
8. Liu J, Bressan M, Hassel D, Huisken J, Staudt D, Kikuchi K, Poss KD, Mikawa T, Stainier DY. A dual role for ErbB2 signaling in cardiac trabeculation. *Development.* 2010;137:3867–3875. doi: 10.1242/dev.053736
9. Rasouli SJ, Stainier DYR. Regulation of cardiomyocyte behavior in zebrafish trabeculation by neuregulin 2a signaling. *Nat Commun.* 2017;8:15281. doi: 10.1038/ncomms15281
10. Gassmann M, Casagranda F, Orioli D, Simon H, Lai C, Klein R, Lemke G. Aberrant neural and cardiac development in mice lacking the ErbB4 neuregulin receptor. *Nature.* 1995;378:390–394. doi: 10.1038/378390a0
11. Lee KF, Simon H, Chen H, Bates B, Hung MC, Hauser C. Requirement for neuregulin receptor erbB2 in neural and cardiac development. *Nature.* 1995;378:394–398. doi: 10.1038/378394a0

12. Bersell K, Arab S, Haring B, Kuhn B. Neuregulin1/ErbB4 signaling induces cardiomyocyte proliferation and repair of heart injury. *Cell*. 2009;138:257–270. doi: 10.1016/j.cell.2009.04.060
13. D'Uva G, Aharonov A, Lauriola M, Kain D, Yahalom-Ronen Y, Carvalho S, Weisinger K, Bassat E, Rajchman D, Yifa O, et al. ERBB2 triggers mammalian heart regeneration by promoting cardiomyocyte dedifferentiation and proliferation. *Nat Cell Biol*. 2015;17:627–638. doi: 10.1038/ncb3149
14. Yang X, Arber S, William C, Li L, Tanabe Y, Jessell TM, Birchmeier C, Burden SJ. Patterning of muscle acetylcholine receptor gene expression in the absence of motor innervation. *Neuron*. 2001;30:399–410. doi: 10.1016/s0896-6273(01)00287-2
15. Kisanuki YY, Hammer RE, Miyazaki J, Williams SC, Richardson JA, Yanagisawa M. Tie2-Cre transgenic mice: a new model for endothelial cell-lineage analysis in vivo. *Dev Biol*. 2001;230:230–242. doi: 10.1006/dbio.2000.0106
16. Del Monte-Nieto G, Ramialison M, Adam AAS, Wu B, Aharonov A, D'Uva G, Bourke LM, Pitulescu ME, Chen H, de la Pompa JL, et al. Control of cardiac jelly dynamics by NOTCH1 and NRG1 defines the building plan for trabeculation. *Nature*. 2018;557:439–445. doi: 10.1038/s41586-018-0110-6
17. Liberzon A, Birger C, Thorvaldsdottir H, Ghandi M, Mesirov JP, Tamayo P. The Molecular Signatures Database (MSigDB) hallmark gene set collection. *Cell Syst*. 2015;1:417–425. doi: 10.1016/j.cels.2015.12.004
18. Harris SL, Levine AJ. The p53 pathway: positive and negative feedback loops. *Oncogene*. 2005;24:2899–2908. doi: 10.1038/sj.onc.1208615
19. Nakayama K, Ishida N, Shirane M, Inomata A, Inoue T, Shishido N, Horii I, Loh DY, Nakayama K. Mice lacking p27(Kip1) display increased body size, multiple organ hyperplasia, retinal dysplasia, and pituitary tumors. *Cell*. 1996;85:707–720. doi: 10.1016/s0092-8674(00)81237-4
20. Passer D, van de Vrugt A, Atmanli A, Domian IJ. Atypical protein kinase C-dependent polarized cell division is required for myocardial trabeculation. *Cell Rep*. 2016;14:1662–1672. doi: 10.1016/j.celrep.2016.01.030
21. McCaffrey LM, Macara IG. Signaling pathways in cell polarity. *Cold Spring Harb Perspect Biol*. 2012;4:a009654. doi: 10.1101/cshperspect.a009654
22. Hikita T, Mirzapourshafiyi F, Barbacena P, Riddell M, Pasha A, Li M, Kawamura T, Brandes RP, Hirose T, Ohno S, et al. PAR-3 controls endothelial planar polarity and vascular inflammation under laminar flow. *EMBO Rep*. 2018;19:e45253. doi: 10.15252/embr.201745253
23. Jimenez-Amilburu V, Stainier DYR. The transmembrane protein Crb2a regulates cardiomyocyte apicobasal polarity and adhesion in zebrafish. *Development*. 2019;146:dev171207. doi: 10.1242/dev.171207
24. di Pietro F, Echard A, Morin X. Regulation of mitotic spindle orientation: an integrated view. *EMBO Rep*. 2016;17:1106–1130. doi: 10.15252/embr.201642292
25. Cherian AV, Fukuda R, Augustine SM, Maischein HM, Stainier DY. N-cadherin relocalization during cardiac trabeculation. *Proc Natl Acad Sci USA*. 2016;113:7569–7574. doi: 10.1073/pnas.1606385113
26. Wang Y, Nakayama M, Pitulescu ME, Schmidt TS, Bochenek ML, Sakakibara A, Adams S, Davy A, Deutsch U, Luthi U, et al. Ephrin-B2 controls VEGF-induced angiogenesis and lymphangiogenesis. *Nature*. 2010;465:483–486. doi: 10.1038/nature09002
27. Travisano SI, Oliveira VL, Prados B, Grego-Bessa J, Pineiro-Sabaris R, Bou V, Gomez MJ, Sanchez-Cabo F, MacGrogan D, de la Pompa JL. Coronary arterial development is regulated by a Dll4-Jag1-EphrinB2 signaling cascade. *Elife*. 2019;8:1–30. doi: 10.7554/eLife.49977
28. Claxton S, Kostourou V, Jadeja S, Chambon P, Hodivala-Dilke K, Fruttiger M. Efficient, inducible Cre-recombinase activation in vascular endothelium. *Genesis*. 2008;46:74–80. doi: 10.1002/dvg.20367
29. Haskins JW, Nguyen DX, Stern DF. Neuregulin 1-activated ERBB4 interacts with YAP to induce Hippo pathway target genes and promote cell migration. *Sci Signal*. 2014;7:ra116. doi: 10.1126/scisignal.2005770
30. Lavoie H, Gagnon J, Therrien M. ERK signalling: a master regulator of cell behaviour, life and fate. *Nat Rev Mol Cell Biol*. 2020;21:607–632. doi: 10.1038/s41580-020-0255-7
31. Payne SR, Zhang S, Tsuchiya K, Moser R, Gurley KE, Longton G, deBoer J, Kemp CJ. p27kip1 deficiency impairs G2/M arrest in response to DNA damage, leading to an increase in genetic instability. *Mol Cell Biol*. 2008;28:258–268. doi: 10.1128/MCB.01536-07
32. Stanley EG, Biben C, Elefanty A, Barnett L, Koentgen F, Robb L, Harvey RP. Efficient Cre-mediated deletion in cardiac progenitor cells conferred by a 3'UTR-ires-Cre allele of the homeobox gene Nkx2-5. *Int J Dev Biol*. 2002;46:431–439.
33. Goodyer WR, Beyersdorf BM, Paik DT, Tian L, Li G, Buikema JW, Chirikian O, Choi S, Venkatraman S, Adams EL, et al. Transcriptomic profiling of the developing cardiac conduction system at single-cell resolution. *Circ Res*. 2019;125:379–397. doi: 10.1161/CIRCRESAHA.118.314578
34. Rentschler S, Zander J, Meyers K, France D, Levine R, Porter G, Rivkees SA, Morley GE, Fishman GI. Neuregulin-1 promotes formation of the murine cardiac conduction system. *Proc Natl Acad Sci USA*. 2002;99:10464–10469. doi: 10.1073/pnas.162301699
35. Redmond CJ, Coulombe PA. Intermediate filaments as effectors of differentiation. *Curr Opin Cell Biol*. 2021;68:155–162. doi: 10.1016/j.ceb.2020.10.009
36. Blagosklonny MV. Cell senescence and hypermitogenic arrest. *EMBO Rep*. 2003;4:358–362. doi: 10.1038/sj.embor.embor806
37. Hnit SS, Xie C, Yao M, Holst J, Bensoussan A, De Souza P, Li Z, Dong Q. p27(Kip1) signaling: transcriptional and post-translational regulation. *Int J Biochem Cell Biol*. 2015;68:9–14. doi: 10.1016/j.biocel.2015.08.005
38. Ya J, Markman MW, Wagenaar GT, Blommaart PJ, Moorman AF, Lamers WH. Expression of the smooth-muscle proteins alpha-smooth-muscle actin and calponin, and of the intermediate filament protein desmin are parameters of cardiomyocyte maturation in the prenatal rat heart. *Anat Rec*. 1997;249:495–505. doi: 10.1002/(SICI)1097-0185(199712)249:4<495::AID-AR9>3.0.CO;2-Q
39. Clarke DN, Martin AC. Actin-based force generation and cell adhesion in tissue morphogenesis. *Curr Biol*. 2021;31:R667–R680. doi: 10.1016/j.cub.2021.03.031
40. Aharonov A, Shakked A, Umansky KB, Savidor A, Genzelinakh A, Kain D, Lendengolts D, Revach OY, Morikawa Y, Dong J, et al. ERBB2 drives YAP activation and EMT-like processes during cardiac regeneration. *Nat Cell Biol*. 2020;22:1346–1356. doi: 10.1038/s41556-020-00588-4
41. Grundl M, Walz S, Hauf L, Schwab M, Werner KM, Spahr S, Schulte C, Maric HM, Ade CP, Gaubatz S. Interaction of YAP with the Myb-MuvB (MMB) complex defines a transcriptional program to promote the proliferation of cardiomyocytes. *PLoS Genet*. 2020;16:e1008818. doi: 10.1371/journal.pgen.1008818
42. Pattschull G, Walz S, Grundl M, Schwab M, Ruhl E, Baluapuri A, Cindric-Vranesic A, Kneitz S, Wolf E, Ade CP, et al. The Myb-MuvB complex is required for YAP-dependent transcription of mitotic genes. *Cell Rep*. 2019;27:3533–3546.e7. doi: 10.1016/j.celrep.2019.05.071
43. Monroe TO, Hill MC, Morikawa Y, Leach JP, Heallen T, Cao S, Krijger PHL, de Laat W, Wehrens XHT, Rodney GG, et al. YAP partially reprograms chromatin accessibility to directly induce adult cardiogenesis in vivo. *Dev Cell*. 2019;48:765–779.e7. doi: 10.1016/j.devcel.2019.01.017
44. Yang S, Zhang L, Liu M, Chong R, Ding SJ, Chen Y, Dong J. CDK1 phosphorylation of YAP promotes mitotic defects and cell motility and is essential for neoplastic transformation. *Cancer Res*. 2013;73:6722–6733. doi: 10.1158/0008-5472.CAN-13-2049
45. Staudt DW, Liu J, Thorn KS, Stuurman N, Liebling M, Stainier DY. High-resolution imaging of cardiomyocyte behavior reveals two distinct steps in ventricular trabeculation. *Development*. 2014;141:585–593. doi: 10.1242/dev.098632
46. Barak Y, Hemberger M, Sucov HM. Phases and mechanisms of embryonic cardiomyocyte proliferation and ventricular wall morphogenesis. *Pediatr Cardiol*. 2019;40:1359–1366. doi: 10.1007/s00246-019-02164-6
47. Gupta V, Poss KD. Clonally dominant cardiomyocytes direct heart morphogenesis. *Nature*. 2012;484:479–484. doi: 10.1038/nature11045
48. Yang J, Antin P, Berx G, Blanpain C, Brabletz T, Bronner M, Campbell K, Cano A, Casanova J, Christofori G, et al; EMT International Association (TEMTIA). Guidelines and definitions for research on epithelial-mesenchymal transition. *Nat Rev Mol Cell Biol*. 2020;21:341–352. doi: 10.1038/s41580-020-0237-9
49. Tang N, Marshall WF, McMahon M, Metzger RJ, Martin GR. Control of mitotic spindle angle by the RAS-regulated ERK1/2 pathway determines lung tube shape. *Science*. 2011;333:342–345. doi: 10.1126/science.1204831
50. Tang N, Marshall WF. Centrosome positioning in vertebrate development. *J Cell Sci*. 2012;125:4951–4961. doi: 10.1242/jcs.038083
51. Tian X, Li Y, He L, Zhang H, Huang X, Liu Q, Pu W, Zhang L, Li Y, Zhao H, et al. Identification of a hybrid myocardial zone in the mammalian heart after birth. *Nat Commun*. 2017;8:87. doi: 10.1038/s41467-017-00118-1
52. LeGoff L, Lecuit T. Mechanical forces and growth in animal tissues. *Cold Spring Harb Perspect Biol*. 2015;8:a019232. doi: 10.1101/cshperspect.a019232
53. Musacchio A, Salmon ED. The spindle-assembly checkpoint in space and time. *Nat Rev Mol Cell Biol*. 2007;8:379–393. doi: 10.1038/nrm2163
54. Jones MC, Zha J, Humphries MJ. Connections between the cell cycle, cell adhesion and the cytoskeleton. *Philos Trans R Soc Lond B Biol Sci*. 2019;374:20180227. doi: 10.1098/rstb.2018.0227
55. Gachet Y, Tournier S, Millar JB, Hyams JS. A MAP kinase-dependent actin checkpoint ensures proper spindle orientation in fission yeast. *Nature*. 2001;412:352–355. doi: 10.1038/35085604
56. Yan Y, Black CP, Cowan KH. Irradiation-induced G2/M checkpoint response requires ERK1/2 activation. *Oncogene*. 2007;26:4689–4698. doi: 10.1038/sj.onc.1210268
57. Lin Z, von Gise A, Zhou P, Gu F, Ma Q, Jiang J, Yau AL, Buck JN, Gouin KA, van Gorp PR, et al. Cardiac-specific YAP activation improves cardiac function

and survival in an experimental murine MI model. *Circ Res*. 2014;115:354–363. doi: 10.1161/CIRCRESAHA.115.303632
58. Morikawa Y, Zhang M, Heallen T, Leach J, Tao G, Xiao Y, Bai Y, Li W, Willerson JT, Martin JF. Actin cytoskeletal remodeling with protrusion formation is essential for heart regeneration in Hippo-deficient mice. *Sci Signal*. 2015;8:ra41. doi: 10.1126/scisignal.2005781
59. Finsterer J, Stollberger C, Towbin JA. Left ventricular noncompaction cardiomyopathy: cardiac, neuromuscular, and genetic factors. *Nat Rev Cardiol*. 2017;14:224–237. doi: 10.1038/nrcardio.2016.207
60. Kodo K, Ong SG, Jahanbani F, Termglinchan V, Hirono K, InanlooRahatloo K, Ebert AD, Shukla P, Abilez OJ, Churko JM, et al. iPSC-derived cardiomyocytes reveal abnormal TGF-beta signalling in left ventricular non-compaction cardiomyopathy. *Nat Cell Biol*. 2016;18:1031–1042. doi: 10.1038/ncb3411
61. Luxan G, Casanova JC, Martinez-Poveda B, Prados B, D'Amato G, MacGrogan D, Gonzalez-Rajal A, Dobarro D, Torroja C, Martinez F, et al. Mutations in the NOTCH pathway regulator MIB1 cause left ventricular noncompaction cardiomyopathy. *Nat Med*. 2013;19:193–201. doi: 10.1038/nm.3046
62. Soriano P. Generalized lacZ expression with the ROSA26 Cre reporter strain. *Nat Genet*. 1999;21:70–71. doi: 10.1038/5007
63. Kanzler B, Kuschert SJ, Liu YH, Mallo M. Hoxa-2 restricts the chondrogenic domain and inhibits bone formation during development of the branchial area. *Development*. 1998;125:2587–2597. doi: 10.1242/dev.125.14.2587
64. Gonzalez-Costa T, de la Pompa JL, Grego-Bessa J. En face endocardial cushion preparation for planar morphogenesis analysis in mouse embryos. *J Vis Exp*. 2022;(185):e64207. doi: 10.3791/64207
65. Mukouyama YS, James J, Nam J, Uchida Y. Whole-mount confocal microscopy for vascular branching morphogenesis. *Methods Mol Biol*. 2012;843:69–78. doi: 10.1007/978-1-61779-523-7_7
66. Li B, Dewey CN. RSEM: accurate transcript quantification from RNA-seq data with or without a reference genome. *BMC Bioinf*. 2011;12:323. doi: 10.1186/1471-2105-12-323
67. Robinson MD, McCarthy DJ, Smyth GK. edgeR: a bioconductor package for differential expression analysis of digital gene expression data. *Bioinformatics*. 2010;26:139–140. doi: 10.1093/bioinformatics/btp616
68. Metsalu T, Vilo J. ClustVis: a web tool for visualizing clustering of multivariate data using principal component analysis and heatmap. *Nucleic Acids Res*. 2015;43:W566–W570. doi: 10.1093/nar/gkv468
69. Subramanian A, Tamayo P, Mootha VK, Mukherjee S, Ebert BL, Gillette MA, Paulovich A, Pomeroy SL, Golub TR, Lander ES, et al. Gene set enrichment analysis: a knowledge-based approach for interpreting genome-wide expression profiles. *Proc Natl Acad Sci USA*. 2005;102:15545–15550. doi: 10.1073/pnas.0506580102
70. Thomas PD, Ebert D, Muruganujan A, Mushayahama T, Albou LP, Mi H. PANTHER: making genome-scale phylogenetics accessible to all. *Protein Sci*. 2022;31:8–22. doi: 10.1002/pro.4218